APPLICATION OF LIQUID-LIQUID INTERACTIONS WITH SINGLE-WALLED CARBON NANOTUBES

By

RANDY KAI-WEI WANG

A DISSERTATION PRESENTED TO THE GRADUATE SCHOOL
OF THE UNIVERSITY OF FLORIDA IN PARTIAL FULFILLMENT
OF THE REQUIREMENTS FOR THE DEGREE OF
DOCTOR OF PHILOSOPHY

UNIVERSITY OF FLORIDA

2009

To my family in Taiwan, who, always support all my efforts especially for my PhD

ACKNOWLEDGMENTS

I sincerely express my gratitude to my advisor, Professor Kirk J. Ziegler, for his technical guidance throughout my graduate research. I will always be grateful for his patience and encouragement. I also thank my committee members, Professor Ranga Narayanan, Professor Peng Jiang, and Professor Ant Ural for their contribution to my proposal presentation and dissertation defense.

I thank our group members, Justin Hill, Carlos Silvera, Fahd Rajab, Wei-Chiang Chen, and Cheng-Yin Lin for giving me lots of suggestion and assistance to my research. I was very fortunate to be a member of this group.

Finally, and most importantly, I express my thanks and gratitude to my parents and friends in Taiwan, who have always supported me in spirit along this journey. I also appreciate my dearest girl friend Jiun-Yi Tsai, who has always been my greatest support during my life in United States. My parents and friends gave me the courage to pursue my dreams, and Jiun-Yi encouraged me to be a successful researcher with an aggressive attitude in life and work. I am always going to be grateful for having them by my side.

TABLE OF CONTENTS

LIST OF TABLES

LIST OF FIGURES

Abstract of Dissertation Presented to the Graduate School
of the University of Florida in Partial Fulfillment of the
Requirements for the Degree of Doctor of Philosophy

APPLICATION OF LIQUID-LIQUID INTERACTIONS WITH SINGLE-WALLED CARBON NANOTUBES

By

Randy Kai-Wei Wang

August 2009

Chair: Kirk J. Ziegler
Major: Chemical Engineering

This study covers three important research topics related to the application of liquid-liquid interaction with single-walled carbon nanotubes (SWNTs). The first topic describes the removal of SWNT bundles from liquid suspensions of nanotubes. The key to this work includes the use of liquid-liquid interfaces to trap the SWNT bundles due to the free energy change of the system during the process.

SWNTs pack into crystalline ropes that form bundles due to strong van der Waals attraction. Bundling diminishes mechanical and electronic properties because it could interrupt the electronic structure of the nanotubes. Also, the electronic devices based on as-grown nanotubes, which contains a mixture of individual nanotubes and nanotube bundles, make the electrical response unpredictable. We developed a new simple process to remove bundles by liquid-liquid interaction. SWNTs bundles are trapped at the interface because bundles stabilize the emulsions. Eliminating the use of ultracentrifugation to remove SWNT bundles enables large-scale production with reduced production costs and time savings.

The second topic presented the swelling effect of the surfactant layer surrounding SWNTs with nonpolar solvents. Solvatochromic shifts in the absorbance and fluorescence spectra are observed when surfactant-stabilized aqueous SWNT suspensions are mixed with immiscible

organic solvents. When aqueous surfactant-suspended SWNTs are mixed with certain solvents, the spectra closely match the peaks for SWNTs dispersed in only that solvent. These spectral changes suggest the hydrophobic region of the micelle surrounding SWNTs swells with the organic solvent when mixed. The solvatochromic shifts of the aqueous SWNT suspensions are reversible once the solvent evaporates. However, some surfactant-solvent systems show permanent changes to the fluorescence emission intensity after exposure to the organic solvent. The intensity of some large diameter SWNT (*n*, *m*) types increase by more than 175%. These differences are attributed to surfactant reorganization, which can improve nanotube coverage, resulting in decreased exposure to quenching mechanisms from the aqueous phase.

The third topic describes the further study of the solvatochromism of the SWNTs. Since SWNTs are encapsulated with microenvironments of nonpolar solvents, it provides a new method to measure the photophysical properties of nanotubes in environments with known properties. Fluorescence and absorbance spectra of SWNTs show solvatochromic shifts in 16 nonpolar solvents, which are proportional to the solvent induction polarization. The photophysical properties of SWNTs were used to determine the relationship between the longitudinal polarizability and other nanotube properties, $\alpha_{11,\|} \propto 1/(R^2 E_{11}{}^3)$.

CHAPTER 1
INTRODUCTION

Single-walled carbon nanotubes (SWNTs) are ultrathin and impressively long macromolecules made of pure carbon with structures as regular and symmetric as crystals. They can be utilized in devices at a molecular scale and offer the possibility of shrinking devices further because the speed, density, and efficiency of devices all rise rapidly as the minimum feature size decreases. SWNTs have a tensile strength 20 times that of steel, carry 1000 times more current density than copper wires, and transport charges down the nanotube without significant scattering. [1] There are approximately 30 different (n, m) types (approx. 1/3 metallic; 2/3 semiconducting) produced in the raw HipCo SWNT materials. The index (n, m) defines the length and angle (α) of the SWNT's roll-up vector on a graphene sheet shown in Figure 1-1. [2] The difference between metallic and semiconducting nanotubes is only small changes in the angle by which the graphene sheet is rolled into a nanotube. Therefore, small changes in α lead to different (n, m) types, resulting in different electrical properties for both metallic and semiconducting types since each different (n, m) has specific energy states.

1.1 The Electronic State of SWNTs

Generally, all nanotubes can be described by the indices $| n - m | = 3q$. If q is an integer, the tubes are assigned as metallic or semimetallic. Otherwise, they are semiconducting nanotubes with geometry-dependent bandgaps. Therefore, each (n, m) type of semiconducting nanotubes generates near-infrared (NIR) fluorescence of a specific wavelength; the intensity of the fluorescence is based on the concentration of each (n, m) semiconducting tube.

The density of electronic states (DOS) describes the number of electronic states at a particular energy and is used to understand the optical transitions of SWNTs. As shown in Figure 1-2, one-dimensional materials, such as SWNTs, show sharp peaks in the DOS, which are called

van Hove singularities and are similar to molecular energy levels. Therefore, optical transitions of SWNTs occur between matching peaks in the 1D DOS. When a SWNT absorbs energy (E_{22}), the electron is excited from the valence band to the conduction band. Then, after the electron loses energy through nonradiative relaxation to the lowest conduction band energy state, the electron recombines with the hole in the valence band, yielding radiative fluorescence emission (E_{11}) (It is also the bandgap of SWNTs). [3] Because the energy states vary for each (n,m) type, E_{11} and E_{22} vary with SWNT diameter.

1.2 Characterization of SWNTs

Most applications employing the unique electronic, thermal, optical, and mechanical properties of individual SWNTs [4-7] and any separation processes will require the large-scale manipulation of stable suspensions at high weight fraction. Individual SWNTs suspensions will bring nanotube science into better contact with fundamental research on self-assembly in complex fluids. Unfortunately, nanotubes bundle easily and are difficult to suspend as a result of substantial van der Waals attractions between tubes. [8] Bundled nanotubes also perturb the electronic structure of semiconducting SWNTs, quenching their intrinsic fluorescence, [2, 9, 10] limiting all attempts to separate the tubes by size or type or to use them as individual macromolecular species.

Generally, optical absorption, [11] NIR fluorescence, [2, 9, 10] and Raman spectroscopy [12] have been the most common measurement techniques to characterize and evaluate the dispersion quality of SWNT suspensions. NIR fluorescence provides direct evidence of the dispersion of individual SWNTs because only individual semiconducting nanotubes emit fluorescence radiation. [9] The Raman Radial Breathing Modes of nanotubes are sensitive to disturbances from their surroundings. Therefore, these modes result in an aggregation peak,

which is measure of the extent of dispersion. [13] In contrast, optical absorption spectroscopy has limited sensitivity to detect the bundling in SWNT suspensions. [14]

The surrounding media of SWNTs can influence the optical measurements, such as absorption and fluorescence, by showing the characteristic peak shifts in spectra. It has been shown that the optical transition energy of SWNTs in various solvents and surfactants shifts to lower energies with increasing dielectric constant of the surrounding media. [15, 16] This environmentally induced energy shift is due to the rearrangement of the media molecules to solvate the dipoles of SWNTs, causing a change in the reaction field. Therefore, each solvent yields unique emission or adsorption spectra called the solvatochromic shift. Investigation of this solvatochromic shift should allow us to understand the photophysics of SWNTs in different dielectric environments and help us characterize the surfactant structure surrounding SWNTs.

1.3 The Surfactant Structure on SWNTs

SWNTs can be dispersed in aqueous media when coated by adsorbed surfactants. This simple non-covalent method is able to disperse both organic and inorganic particles since the hydrophilic head groups help particles with limited solubility disperse homogeneously in an aqueous solution. Sodium dodecyl sulfate (SDS) and sodium dodecylbenzene sulfonate (SDBS) are commonly used ionic surfactants to generate high quality dispersions of individual SWNTs due to the electrostatic repulsion. O'Connell et al. [9] have suggested that SDS forms a cylindrical structure around nanotubes. Others have shown that either a hemimicellar [17] or random distribution of SDS surfactant forms on the nanotubes without preferential arrangement of the head and tail groups when the surfactants adsorb on the sidewall of SWNTs . [18] Figure 1-3 shows the schematic representation of possible adsorption structures of SDS surfactants. [18]

Nonionic surfactants such as natural [19] and artificial polymers [15] are also used to produce SWNT suspensions. These two kinds of surfactant have bulky hydrophilic groups that

are able to prevent the aggregation of nanotubes due to the enhanced steric stabilization provided by longer polymeric groups. However, the real surfactant structure remains unknown whenever the ionic or nonionic surfactants are used. Wallace et al. [20] have suggested that the concentration of surfactant determines the mechanism of adsorption on the SWNTs. They have also suggested that the chirality of the SWNTs can influence the wrapping angle of the surfactants on the SWNT at low concentration. Therefore, it is clear that the concentration of surfactants, which affect the micelle structure, plays an important role on understanding the dispersion mechanism of the SWNT in the aqueous media.

1.4 Pickering Emulsions

Nanoparticles, such as SWNTs, can not only be suspended by the surfactant but also act as surfactants to stabilize the emulsions. These particle-stabilized emulsions, also known as Pickering emulsions, [21] are extremely stable and have been used to self-assemble nanoparticles at the liquid-liquid interfaces, [22, 23] to separate the particles, [24] and to prepare unique porous structures. [25] Figure 1-4 is the typical Pickering emulsions stabilized by Gum Arabic-suspended SWNTs. In general, the stability of the Pickering emulsions is determined by the extent to which the particles are wetted by the two immiscible fluids, particle sizes, concentration, and mutual interaction. [26] Particles with higher hydrophilicity (having smaller contact angles θ_{ow}) will preferentially stabilize oil-in-water emulsions, and more hydrophobic particles (having larger contact angles θ_{ow}) will tend to stabilize the water-in-oil emulsions. These emulsions also provide a new route to develop large-scale purification of carbon nanotube suspensions, which is described further in Chapters 2 and 3.

1.5 Bundle Removal and Type Separation of SWNTs

The general method for producing individually suspended nanotubes involves high-shear homogenization, ultrasonication, and ultracentrifugation to remove the SWNT bundles from individual SWNTs. [9] However, ultracentrifugation is not suitable for large-scale production because of its limited scale, high price, and time-consuming process. This leads to negative economic impacts. Therefore, a faster and higher throughput technique to remove nanotube bundles will be required for the successful generation of individual SWNTs for further potential applications.

The mixture of metallic and semiconducting types in raw SWNTs is another drawback for the applications since it limits the performance of devices because devices based on as-grown SWNTs make the electrical response unpredictable. Separation processes offer the possibility of dividing the raw SWNTs material into the metallic and semiconducting nanotubes. Researchers [27] have shown that electrophoresis can be utilized to obtain a degree of separation. Rinzler and coworkers [28] have suggested that the complexation of metallic SWNTs with bromine is able to separate the mixture of tubes in two types. In addition, Zheng et al. [29] have developed the DNA-based chromatography technique to achieve separation. Recently, Density differentiation has also been discovered to sort SWNTs with different electronic structure. [30] Although the methods described above are able to separate SWNT in type, the major problem with these techniques is that they are only analytical-scale techniques. Therefore, a large-scale production of separation method will be necessary to generate specific SWNTs type.

In order to remove the SWNT bundles and enable type separation, liquid-liquid interactions are utilized since it is a low-cost, time-saving and easy-to-scale-up process. As described in Section 1.4, solid particles adsorb at liquid-liquid interfaces stabilizing Pickering emulsions, which can be an appropriate method to remove SWNT bundles. In addition, the

interfaces have high capacities to open a new route for large-scale technique. Hence, it provides an opportunity to remove the bundles dispersed in the aqueous phase from individual tubes.

1.6 Applications of SWNTs

The development of purification and type separation techniques will open up a multitude of applications in the materials science, microelectronic, bionanotechnology, and medical fields. Individual semiconducting SWNTs with specific (n, m) types can be utilized in the construction of microelectronic transistors with known band gaps. Semiconducting SWNTs have been used as a channel through which electron flow in field-effect transistors (FETs) between two metal electrodes with SWNTs as shown in Figure 1-5. The gate electrode can change the conductivity of the nanotube channel in a FET by a factor of one million or more comparable to silicon FETs. Also, because of its nanoscale size, the nanotube FETs should switch reliably using much less power than silicon-based devices. In general, the requirement for the devices is to be made much smaller because they could pack more devices into the same area. However, the problem to limit shrinking metal wires further is that there is still no good way to remove the heat produced by the devices, so packing them in more tightly will only lead to rapid overheating. SWNTs could solve the problem since scientists have found that nanotubes could conduct heat nearly as well as diamond or sapphire. Therefore, nanotubes could efficiently cool very dense arrays of devices.

Individual semiconducting SWNTs were also suggested to be utilized as biosensors to replace traditional dyes suffering from bleaching, degradation, and toxicity problems. [31] They are expected to detect single enzyme or protein molecules accurately, providing high-sensitive biosensing applications. Strano and coworkers [32] have developed a SWNT-based implantable biosensor, which is able to detect the β-D-glucose in solution phase based on their inherent

fluorescent properties. Therefore, the ability to synthesize or separate the SWNTs by type should aid the development of biosensors.

For metallic SWNTs, it can be used as ballistic conductors because they have little electrical resistance which is usually a disadvantage in metal wires. Since electrons can travel long distances without scattering, they can maintain their quantum states. It is also appropriate to utilize them as optical fibers for telecommunication over long distances since the signal will not be decayed. Also, metallic nanotubes can transport electric current greater than 10^9 A/cm^2, which will vaporize metals, such as copper or gold. [33] Metallic SWNTs can also be applied to photovoltaic cells since they can be as conductive transparent electrodes, which are a crucial component in solar cells.

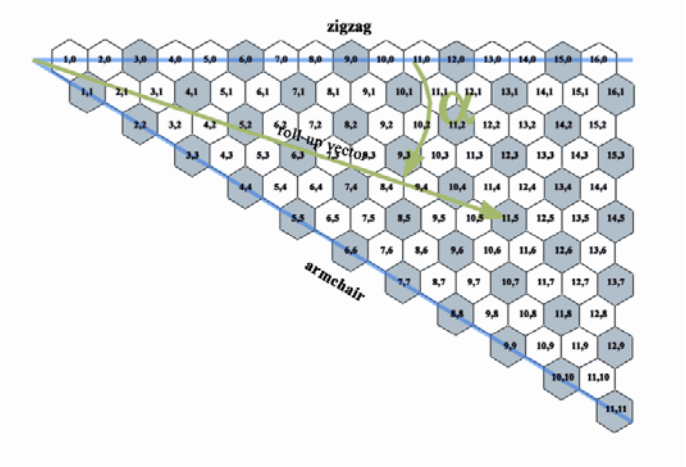

Figure 1-1: SWNTs can be viewed as a grapheme layer wrapped into a tubular structure. The vector connecting two points on the plane can be described by the indices *n* and *m*. [2]

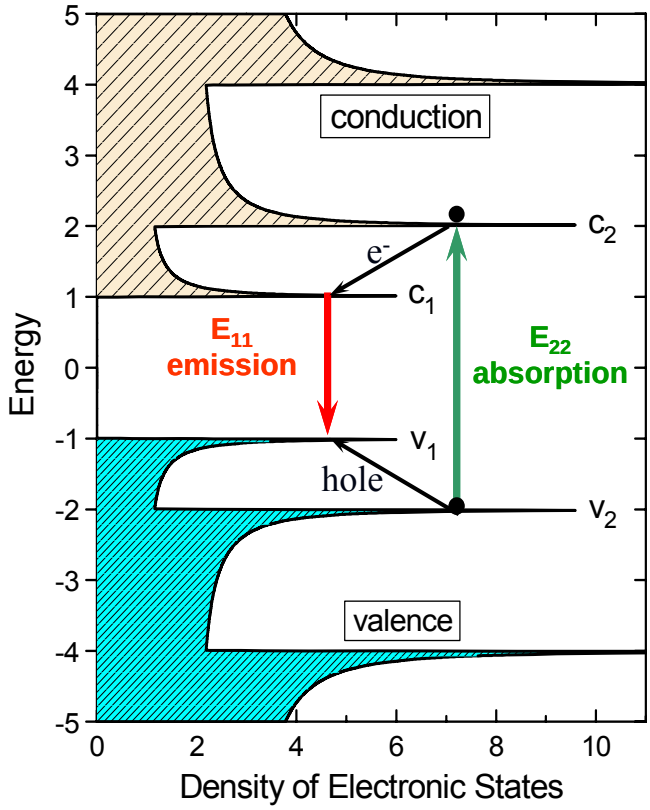

Figure 1-2: Density of electronic states for a single nanotube. Color arrows indicate the optical transitions; black arrows represent the nonradiative relaxation of the electron (in the conduction band) and hole (in the valence band). [2]

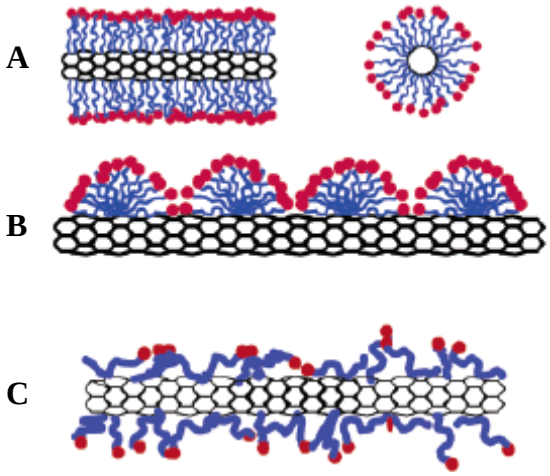

Figure 1-3: Possible adsorption structures of SDS surfactants on a SWNT: A) SWNT encapsulated in a cylindrical structure. B) Hemimicellar structure of SDS surfactants on a SWNT. C) Random distribution of SDS surfactants on a SWNT. [18]

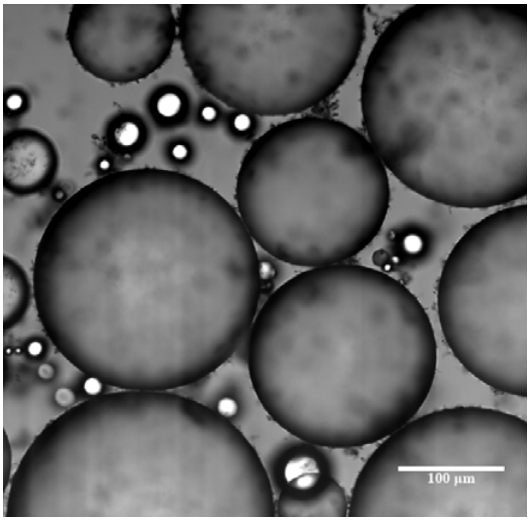

Figure 1-4: Toluene/water emulsions stabilized by surfactant-suspended SWNTs. [34]

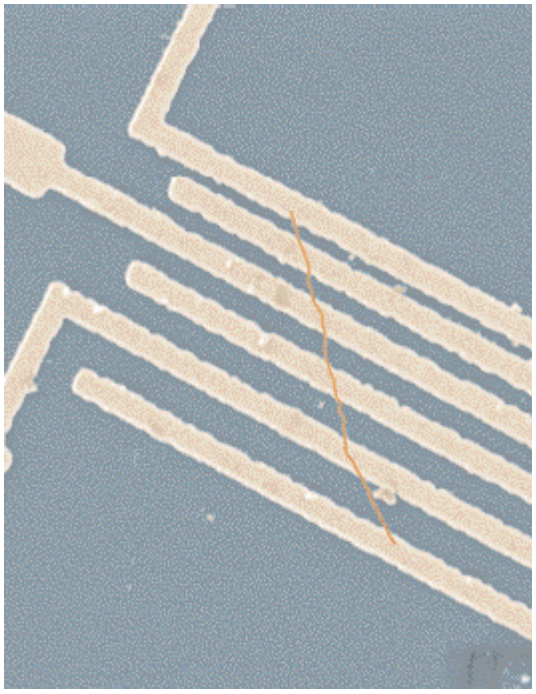

Figure 1-5: The SWNT-based transistor. As ultrathin wires, SWNTs could free up space in microchips for more devices, as well as solving heat and stability problems. At a little over a nanometer in diameter, this SWNT makes lines drawn by state-of-the-art photolithography look huge in comparison. [1]

CHAPTER 2
INTERFACIAL TRAPPING IN REMOVING SWNT BUNDLES

SWNTs pack into bundles because of the strong van der Waals attractive forces. [8, 35] High-energy ultrasonication is often used to overcome these forces to obtain individual SWNTs in solution. However, many common solvents have insufficient solvation forces to suspend SWNTs, yielding low degrees of solubility. [36] These suspensions consist of many small bundles and relatively few individual SWNTs. The difficulties associated with obtaining individually dispersed SWNTs limits nanotube applications, [35, 37, 38] leading researchers to develop a multitude of functionalization schemes to achieve nanotube suspensions. [36, 38-40]

Noncovalent functionalization routes are preferred in many applications to preserve the properties of SWNTs. However, researchers have noted that these approaches yield a solution containing individual nanotubes as well as nanotube bundles. [2] The bundling of nanotubes diminishes the mechanical properties in nanocomposites since the SWNTs slip past one another under stress. [41] Bundled nanotubes also perturb the electronic structure of semiconducting SWNTs, quenching their intrinsic fluorescence. [2, 9, 10] The conventional method to disperse individual nanotubes in aqueous solutions is by high-shear homogenization in various surfactant solutions [15, 19] followed by ultrasonication and ultracentrifugation. [9] However, ultracentrifugation is a time-consuming approach to the removal of SWNT bundles. Therefore, alternative routes to remove bundles from SWNT suspensions are needed for economic, large-scale dispersion.

In this chapter, we describe a simple alternative approach to ultracentrifugation using liquid–liquid interfaces to remove nanotube bundles from the aqueous SWNT suspension. This technique has already been combined with density gradient ultracentrifugation [30] to significantly improve field-effect transistor performance. [42] The adsorption of colloidal

particles at interfaces was first characterized by Pickering in 1907. [21] These systems have been used to self-assemble particles at the interface, [22, 23] to separate particles, such as ampicillin and phenylglycine crystal mixtures in water/alkanol systems, [24, 43] and to prepare unique porous structures. [25] Pickering systems have also demonstrated the large-scale separation of bioparticles, achieving efficiencies greater than centrifugation. [44] Wang, Hobbie and co-workers [45, 46] were the first to show SWNT-based stabilization of emulsions. Bare nanotubes were used as amphiphobic surfactants that stabilized toluene/water emulsions for months. [45] Later, DNA-wrapped SWNTs were shown to stabilize emulsions for the synthesis of colloidal particles. [46] Stabilized emulsions were also seen in length-based separations of functionalized SWNTs. [47] More recently, researchers have begun to use SWNT-based Pickering emulsions for other applications. Asuri et al. [48] demonstrated that interfacial SWNTs decreased transport limits and improved catalytic activity of two-phase reactions leading to increased bioreactivity. Others used polymerization reactions [49, 50] or nanotube interactions [51] to prepare nanotube capsules for supports, controlled release capsules, [51] and lubricating additives. [25]

The method and mechanism of the interfacial trapping process are also provided for removing nanotube bundles from aqueous suspensions. Near-infrared (NIR) fluorescence, vis–NIR absorbance, and Raman spectroscopy as well as atomic force microscopy (AFM) and rheology are used to characterize the SWNT suspensions. New approaches to improve dispersion quality are also discussed. The suspensions prepared by interfacial trapping have comparable dispersion quality to those prepared by ultracentrifugation.

2.1 Experimental Procedure

2.1.1 Dispersion

Nanotube suspensions were prepared with a given initial mass (typically between 6 and 20 mg) of raw SWNTs (Rice HPR 145.1) and mixed with 200 mL of an aqueous Gum Arabic

(Sigma-Aldrich) surfactant solution [19] (1 wt %) to form an initial concentration of 0.03–0.2 mg/mL. High-shear homogenization (IKA T-25 Ultra-Turrax) for 1 h and ultrasonication (Misonix S3000) for 10 min aided dispersion. Control samples were ultracentrifuged at speeds between 20,000 and 26,000 rpm (Beckman Coulter Optima L-80 K) for 4–5 h to remove nanotube bundles.

2.1.2 Interfacial Trapping

Toluene (Acros, 99%) was added to the aqueous SWNT suspension to form a two-phase system. The two-phase system was then shaken vigorously for 30 s to increase interfacial area. Phase separation occurs within 1–2 min; however, the solutions were allowed to settle for 30–60 min to ensure that steady state was achieved for spectroscopy. All experiments were conducted at an organic to aqueous SWNT suspension volume ratio of 0.1 unless otherwise indicated.

2.1.3 Characterization

The aqueous phase was carefully removed after interfacial trapping to prevent further emulsification. The aqueous phase was characterized by vis–NIR absorbance and NIR fluorescence spectra using an Applied NanoFluorescence Nanospectrolyzer (Houston, TX) with excitation from 662 and 784 nm diode lasers. A concentrated Gum Arabic SWNT suspension was homogenized and ultrasonicated and then incrementally diluted with 1 wt % Gum Arabic solution to determine the linear regions of the absorbance and fluorescence spectra (Figures A-1 (A) and A-1 (B) in the Appendix A). Raman spectra were recorded using a Renishaw Invia Bio Raman with excitation from a 785 nm diode laser. SWNT suspensions were also spin-coated onto mica to collect AFM images on a Digital Instruments Dimension 3100. Diameter analysis was then performed using SIMAGIS software. [52] A minimum of 700 nanotubes were measured for statistically relevant results. The rheology of SWNT suspensions was examined using an ARES LS^{-1} strain-controlled rheometer (TA Instruments). A cone and plate fixture with

a diameter of 50 mm and an angle of 0.04 rad was used to measure the steady shear viscosity at rates between 1 and 100 s^{-1}. As an additional step in preparing the interfacial trapped samples for rheological characterization, the Gum Arabic solution was initially centrifuged at 26000 rpm for 30 min before adding nanotubes. Solutions of Gum Arabic, prior to centrifugation, showed variations in rheology, consistent with other reports. [53, 54] The additional processing produced a stable solution of Gum Arabic with a viscosity of 1.68 ± 0.05 cP as measured over the entire range of shear rates. For rheological characterization, SWNT suspensions were ultracentrifuged for 2 h to prepare similar final concentrations for analysis (determined using the extinction coefficient [55] and absorbance at 763 nm).

2.2 Results and Discussion

2.2.1 Selective Separation of Bundles

After mixing toluene with a homogenized and ultrasonicated aqueous suspension, the system forms a homogeneous gray solution of emulsions. An interphase of emulsions and a bulk aqueous phase forms within a minute as seen in the inset of Figure 2-1. Absorbance spectra of the bulk aqueous phase are shown in Figure 2-1 (A). The homogenized and ultrasonicated sample (control) has high absorbance due to the concentration of both individual (as evidenced by the interband transition peaks) and bundled SWNTs. The absorbance of the suspension has clearly decreased after interfacial trapping while the spectral features have blue-shifted and are better resolved. These changes indicate the removal of nanotubes from the aqueous phase and a higher fraction of individual SWNTs. [56] When the control suspension is ultracentrifuged, the absorbance of the aqueous phase is significantly lower demonstrating that ultracentrifugation removes a significant portion of the nanotubes (both bundled and individual) at the relatively low concentrations used here.

Fluorescence spectra of the aqueous phase are shown in Figure 2-1 (B). For comparison, the spectra after homogenization and ultrasonication are shown (control) as well as the spectra using conventional ultracentrifugation rather than interfacial trapping. The spectra show that ultracentrifugation results in a decrease in fluorescence intensity indicative of the removal of individual nanotubes. However, the fluorescence intensity after interfacial trapping increases when compared to the control sample. It is also important to note that the peak positions for both the interfacial trapped and ultracentrifuged suspensions are identical, indicating that the environment surrounding the nanotube has not changed after mixing with the solvent.

Fluorescence intensities are related to the concentration of individual nanotubes. Fluorescence spectra also provide a sensitive probe to the aggregation state of the aqueous phase. [9, 14] Typically, higher intensity peaks in the spectra indicate better dispersion quality [14] since energy transfer can occur between adjacent nanotubes in bundles resulting in either intensity changes or complete quenching of the fluorescence. [2, 10] This energy transfer mechanism can also occur between individual SWNTs. Several groups [57-59] have observed that energy transfer between SWNTs results in fluorescence changes. The fluorescence intensity of individually suspended SWNTs may decay as the volume fraction increases as observed in solid composites. [60] Concentrated SWNT suspensions could also potentially reabsorb emitted photons thereby reducing the measured emission intensity. However, the dilute initial SWNT concentration (0.03 mg/mL) is in the linear region of both fluorescence and absorbance measurements (see Figures A-1 (A) and A-1 (B) in the Appendix A). Therefore, the increase in fluorescence intensity observed in Figure 2-1 (B) is likely due to reduced quenching after interfacial trapping. Removal of nanotubes from the solution, especially SWNT bundles that

quench fluorescence, would allow more individual, semiconducting SWNTs to emit photons, resulting in increased fluorescence intensities.

SWNT suspensions with a much lower concentration were used during interfacial trapping (0.005 mg/mL) to test whether the enhancement of the fluorescence seen in Figure 2-1 was due to the removal of SWNT bundles. The lower initial concentration results in fewer collisions between nanotubes and, thus, fewer potential quenching events. At these concentrations, changes to the number of quenching bundles in the suspension should have a reduced effect on the spectra. Figure 2-2 (A) shows that fluorescence at low concentrations has only a slight change after interfacial trapping, whereas the absorbance in Figure 2-2 (B) has diminished significantly. Since the fluorescence remains relatively constant, the clear decrease in absorbance can only be attributed to the removal of bundles or other carbonaceous impurities from the aqueous phase, suggesting that selective bundle removal occurs.

2.2.2 Dispersion Quality

Quantifying the fraction of individually suspended SWNTs or bundles in an aqueous solution remains difficult. [14] Rheology, [14, 55] fluorescence, [9, 10, 14] Raman, [14, 61] absorbance, [56] and small-angle neutron scattering (SANS) [14, 46, 62, 63] have already been successfully used to study the interactions of surfactant-coated SWNTs in aqueous solutions. Visual methods such as AFM are also used to obtain qualitative and quantitative information about the dispersion. [17, 52] The group from NIST recommended that multiple techniques be used to quantify dispersion. [14] Several techniques that describe the dispersion quality of the aqueous suspension after interfacial trapping are discussed below. A higher initial SWNT concentration of 0.2 mg/mL was used to investigate the dispersion quality, and the results are summarized in Table 2-1.

The relative intensity of the interband transition peaks in the absorbance spectra and their width are related to the dispersion quality. [9, 14, 56] Tan and Resasco [56] showed that the resonance ratio could be used to characterize the fraction of individual SWNTs in solution. This ratio is calculated by comparing the area for the resonant band with the nonresonant band (carbonaceous impurities and π-plasmon). The interfacial trapping method shows improved dispersion characteristics and improved fractions of individually suspended SWNTs.

Figure 2-3 (A) is the Raman spectra of the SWNT radial breathing modes (RBMs). The peak at ~270 cm^{-1} represents the shift of (10, 2) nanotubes due to bundling, providing a measure of the extent of nanotube aggregation. [13] The homogenized and ultrasonicated suspension has a very intense aggregation peak in comparison to the (11, 3) nanotubes at ~234 cm^{-1}. As seen in Figure 2-3 and Table 2-1, the ratio of these peaks drops dramatically after interfacial trapping, indicating removal of bundled SWNTs.

Figure 2-3 (B) compares the steady values of the shear viscosities for the three different SWNT suspensions. The viscosity of all systems nearly matches at the highest shear rate of 100 s^{-1}, demonstrating that the small difference in concentration across the three systems has a limited impact on the results. Differences in the rheology are apparent at lower shear rates. Except for the lowest shear rate, the control sample has a nearly constant viscosity as a function of shear rate. The ultracentrifugation and interfacial trapping methods produce samples that shear thin. The decrease in viscosity with increasing shear rate is more pronounced for the ultracentrifugation sample but agrees within measurement error with the result from the sample prepared using interfacial trapping. The favorable comparison implies that our method produces a suspension of nanotubes similar in flow characteristics, and hence dispersion quality, to the ultracentrifugation method.

Parts a and b of Figure 2-4 show AFM images of the homogenized and ultrasonicated SWNT suspension compared to the suspension after interfacial trapping while the corresponding histograms of nanotube diameters are shown in Figure 2-4 (C). As expected, the homogenized and ultrasonicated SWNT suspension has many bundled SWNTs and some individually suspended SWNTs (diameters less than ~3 nm), yielding a broad diameter distribution with an average of 12.8 nm. After interfacial trapping, the suspension has significantly fewer bundled SWNTs and a sharper distribution in diameters with an average of 4.1 nm.

The fluorescence intensity provides a measure of the concentration of individually suspended SWNTs but does not account for variations in total concentration (i.e. fraction of individual SWNTs). On the other hand, the absorbance provides an overall measure of the entire ensemble of individual and bundled SWNTs, providing a means of normalizing the fluorescence intensity. The ratio of fluorescence to absorbance (F/A), therefore, is another measure of dispersion quality. This ratio should be the most relevant measurement to many applications since it is related to the quantum yield of the nanotube suspension. Note that this ratio is not a quantitative measure of the fraction of individual SWNTs and it should only be used to compare dispersion characteristics between samples. In this study, the intensity from the (7, 6) nanotube is used and divided by the absorbance at the excitation wavelength (662 nm). The decrease in absorbance and increase in fluorescence cause the F/A ratio to improve after interfacial trapping as shown in Table 2-1.

2.2.3 Improving Separation Effectiveness

In summary, the SWNT suspension resulting from a single-step interfacial trapping process has improved dispersion quality in comparison to homogenized and ultrasonicated suspensions as shown in Table 2-1. SWNT dispersions prepared by ultracentrifugation have higher dispersion quality, but one of the benefits of the interfacial trapping method is that the

process can be easily adjusted to change separation efficiency. Figure 2-5 shows the variation of fluorescence emission intensity of the most prominent (7, 6) nanotube type in the spectra as a function of the volume ratio of toluene to the aqueous SWNT suspension ($R = V_{toluene} / V_{aqueous}$). As seen in Figure 2-5 (A) for an initial SWNT mass concentration of 0.03 mg/mL, higher fluorescence intensity is observed for $R \geq 1$. The higher conductivity of the solution when $R > 1$ suggests that water-in-oil (w/o) emulsions are formed while oil-in-water (o/w) emulsions are seen for $R < 1$. It is also seen that the fluorescence intensity is always greater than the control for initial mass loadings of 0.03 mg/mL. Figure 2-5 (B) shows the fluorescence intensity from an initial mass loading of 0.005 mg/mL of SWNTs. As can be seen in the figure, the emission intensity tends to be lower than the control for o/w emulsions, whereas w/o emulsions show relatively constant intensity. The same trends are seen for other emission peaks and other initial mass loadings (not shown).

Although the fluorescence intensity changes are relatively minor, the changes to the absorbance spectra in Figure 2-6 (A) are significant. The absorbance spectra for all volume ratios have decreased significantly after interfacial trapping when compared to the control sample in Figure 2-1. The interband transition peaks are noticed for all aqueous solutions, indicating good dispersion. The absorption decreases steadily as the volume ratio is reduced and the system shifts from w/o to o/w emulsions. The lowest absorption intensities are seen for o/w systems at a volume ratio of $R = 0.5$. Figure 2-6 (B) plots the F/A ratio as a function of the volume ratio. Higher F/A ratios are seen for o/w systems when compared to w/o systems indicating that a higher fraction of individual nanotubes are suspended in o/w systems via interfacial trapping.

To further improve the quality of the suspensions, a second interfacial trapping step was introduced. The SWNT suspension was first mixed with toluene at a volume ratio of $R = 0.1$

since o/w emulsions were the most effective at removing bundled nanotubes from the aqueous phase. The aqueous phase was separated from the oil and interphase and then mixed again with toluene at a volume ratio of $R = 0.1$. As seen in Figure 2-7 (A), the second interfacial trap has little effect on the fluorescence intensity. However, the absorbance spectrum shown in Figure 2-7 (B) has decreased significantly, resulting in significant changes to the fraction of bundled SWNTs (see Figure A-2 (A) in the Appendix A). The Raman aggregation peak has also shown further improvement after the second interfacial trapping step as shown in Figure 2-7 (C). It is important to note that changes to both Raman and absorbance spectra without changes to the fluorescence provide strong evidence that the interfacial trapping process is highly selective in the removal of bundled SWNTs from the aqueous phase. Table 2-1 summarizes the dispersion quality measurements for the two-step interfacial process compared to ultracentrifugation. As seen in the table, interfacial trapping shows better dispersion than ultracentrifugation by the F/A ratio and comparable dispersion quality when characterized by Raman and absorbance spectra.

2.3 Mechanism

Figure 2-8 shows a conceptual diagram of the overall two-phase interfacial trapping process based on experimental observations. First, nanotubes are homogenized and ultrasonicated in a surfactant solution resulting in a suspension that contains both individually dispersed and bundled SWNTs. An immiscible organic solvent is added to the aqueous suspension forming a two-phase system. This two-phase system is then mixed resulting in emulsions (either o/w or w/o depending on the volume ratios) as shown previously. [34] SWNT bundles preferentially adsorb at the emulsion interface when mixed. The emulsions then coalesce into a continuous phase with some emulsions being stabilized by the SWNT bundles. Finally, phase separation into an organic phase, an interphase of stabilized emulsions, and a transparent aqueous phase allows easy collection of the individually suspended SWNTs.

Although bundled nanotubes have been removed from the aqueous phase at all volume ratios (see Figures 2-5 and 2-6), the slight decrease in emission intensity for o/w systems indicates that individual SWNTs are removed from the aqueous phase. This conclusion is also confirmed by correcting the absorbance spectra for the nonresonant background (Figure A-2 (B) in the Appendix A). This data suggests that o/w emulsions are more effective in removing nanotubes from the aqueous suspension. The preferential adsorption of hydrophilic silica particles in o/w emulsions was also seen by Binks and co-workers. [26, 64] Adjusting the hydrophilicity of the particles had significant effects on the contact angle and their ability to stabilize the emulsions. The individual and bundled nanotubes are coated with hydrophilic surfactants also providing better stabilization of o/w emulsions and, hence, removal from the aqueous phase. In contrast, individual, Gum Arabic-coated nanotubes do not seem to stabilize w/o interfaces as effectively which results in nanotube bundles being the primary constituent of the interface. This could indicate that the system contains a small fraction of uncoated (hydrophobic) or poorly coated nanotube bundles that stabilize w/o emulsions.

Selective partitioning of SWNT bundles to the interface can be understood by describing the initial driving force of a single nanotube by free energy minimization. These simple models do not account for entropic or kinetic effects but have described interfacial assembly of nanoparticles as small as 2.8 nm. [22, 26, 44, 64, 65] Initially, the nanotubes are dispersed in the aqueous phase as shown in Figure 2-9 (A). If both individual and bundled SWNTs are transferred to the oil–water interface upon mixing, the nanotubes will have a contact angle θ measured into the aqueous phase (see Fig. 2-9 (B)). On the basis of experimental evidence [49] and calculations, [50] SWNTs are expected to orient parallel to the interface. Therefore, the decrease in interfacial area for inserting a cylindrical particle of radius (R_{SWNT} or R_{bundle}) and

length (L) between the oil and water phases is given by the expression, $\Delta A_{ow} = 2RL \sin\theta$, as shown in Figure 2-9 (B). The position of the SWNT at the interface depends on the contact angle and results in a loss of particle interactions with the aqueous phase as well as increased interactions with the oil phase. If the interface is assumed planar and the weight of the nanotube is ignored, the energy change upon inserting the nanotube at the interface is

$$\Delta E = 2\pi RL\left(\frac{2\theta}{360^\circ}\right)\left(\gamma_{po} - \gamma_{pw}\right) - 2RL\gamma_{ow}\sin\theta \qquad (2\text{-}1)$$

where γ_{po}, γ_{pw}, and γ_{ow} are the interfacial tensions at the particle–oil, particle–water, and oil–water interface, respectively. If ΔE is negative as expected for hydrophilic particles, the particle will be in a stable position at the interface. Substituting Young's equation, $\gamma_{po} - \gamma_{pw} = \gamma_{ow}\cos\theta$, into equation, the energy change for inserting a nanotube at the oil–water interface is

$$\Delta E = 2RL\gamma_{ow}\left[\frac{\pi\theta}{180^\circ}\cos\theta - \sin\theta\right] \qquad (2\text{-}2)$$

The contact angle will be similar for individual and bundled nanotubes because of their similar hydrophilicity and γ_{ow} is fixed in the system. Therefore, in aqueous SWNT suspensions, the change in energy of inserting a particle at the interface depends on R and L. As seen in equation, the energy is minimized when particles with larger radius and length are at the interface. For example, it is estimated that ΔE is approximately –200 kT for an individual nanotube and –4500 kT for a bundle of the same length containing 7–10 nanotubes. Note from equation (2-2) that longer SWNTs will be preferentially removed from the suspension. Therefore, these estimates for ΔE are likely the minimum initial driving force since bundles have lengths longer than individual nanotubes. These calculations are in agreement with the experimental results presented above as well as the results of Yi et al., [51] which showed reduced emulsion stabilization for short-length multiwalled nanotubes. The relatively large

negative free energy indicates that both individual and bundled SWNTs prefer to reside at the interface. This explains why o/w emulsions showed decreases in fluorescence intensity in Figure 2-5 (B) and fewer individual SWNTs in the corrected absorbance (see Figures A-2 (A) and A-2 (B) in the Appendix A). On the other hand, there will be a competition for the limited interfacial sites in systems with high initial concentration, where the bundles will be preferred because of the greater driving force.

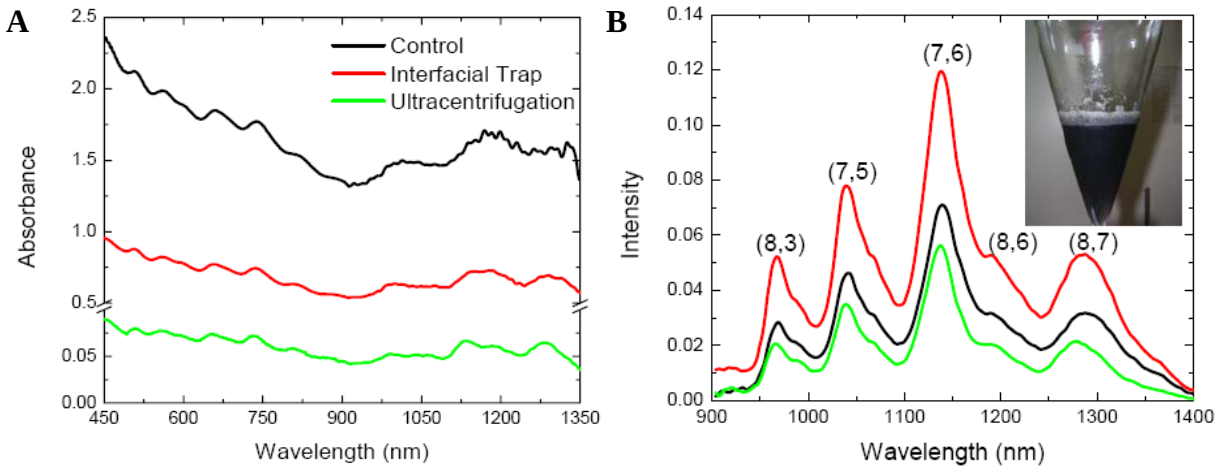

Figure 2-1. A) Absorbance and B) fluorescence (ex = 662 nm) spectra for the interfacial trapping process of Gum Arabic-suspended SWNTs using an initial SWNT mass concentration of 0.03 mg/mL. The control spectra (black lines) are the SWNTs after homogenization and ultrasonication. The inset shows the interfacial trapping process in a separatory funnel. The control sample is then either subjected to ultracentrifugation (green lines) or interfacial traps (red lines). The fluorescence from specific (*n*, *m*) types are labeled.

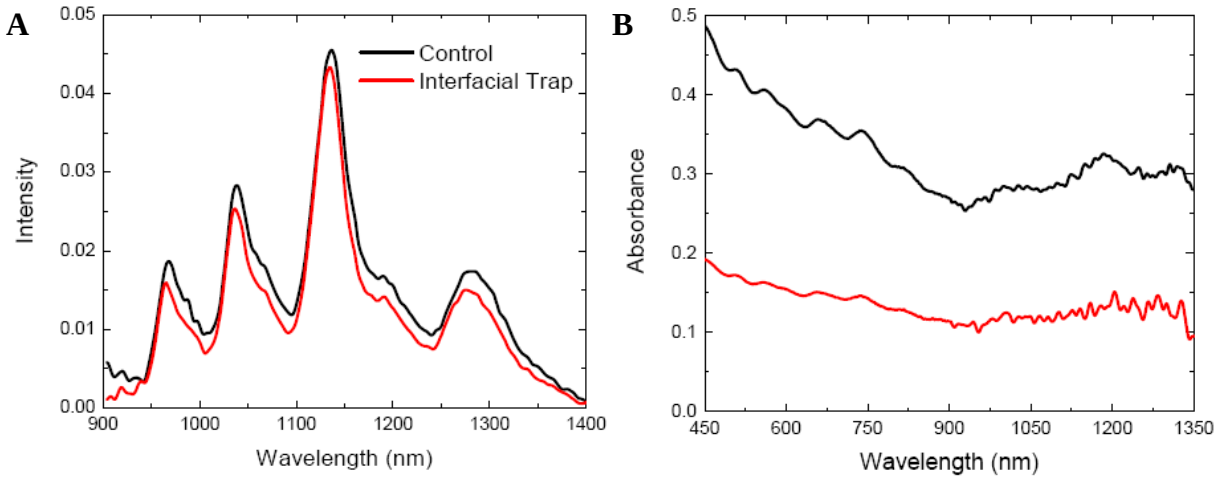

Figure 2-2. A) Absorbance and B) fluorescence (ex = 662 nm) spectra of SWNTs at a concentration of 0.005 mg/mL. The control spectra (black lines) are the SWNTs after homogenization and ultrasonication. The control sample is then subjected to interfacial traps.

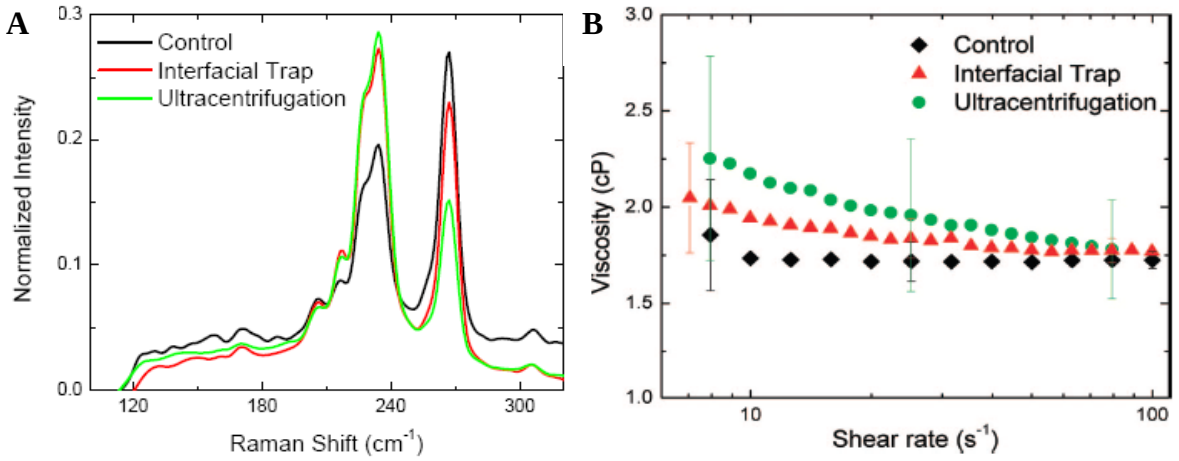

Figure 2-3. A) Normalized Raman spectra of the RBMs (ex = 785 nm) for Gum Arabic-suspended SWNTs after homogenization and ultrasonication (black line), interfacial trapping (red line), and ultracentrifugation (green line). The suspension was prepared from an initial concentration of 0.2 mg/mL raw SWNTs. B) Steady values of the shear viscosities for the Gum Arabic-suspended SWNTs produced after homogenization and ultrasonication (control), interfacial trapping, and ultracentrifugation. The suspensions were prepared at similar concentrations to enable comparison. The final concentration of the control, interfacial trapping suspension, and ultracentrifugation samples were 0.02, 0.026, and 0.025 mg/mL, respectively.

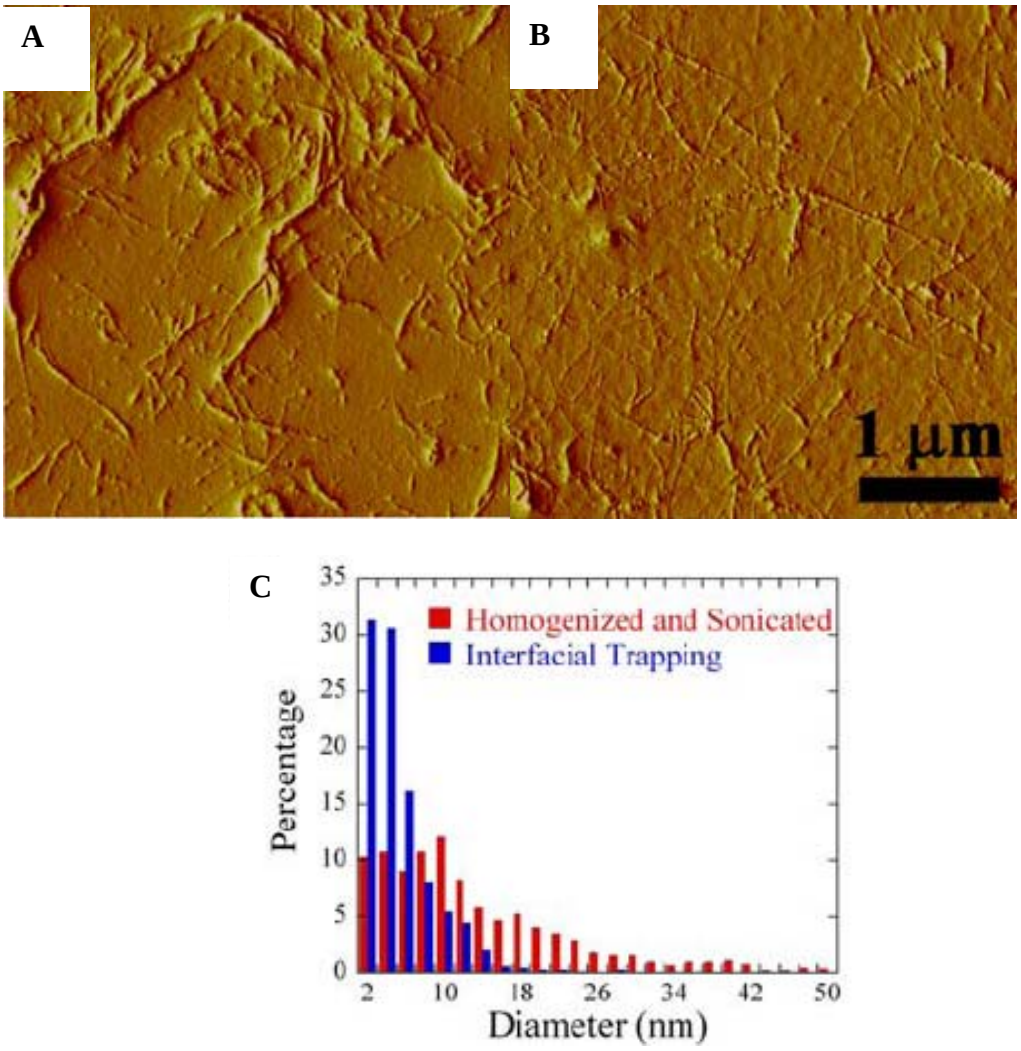

Figure 2-4. AFM images of Gum Arabic SWNT suspensions after A) homogenization and ultrasonication and B) after bundle removal by interfacial trapping. C) Histogram of nanotube diameters measured from the AFM images. The suspension was prepared from an initial concentration of 0.2 mg/mL raw SWNTs.

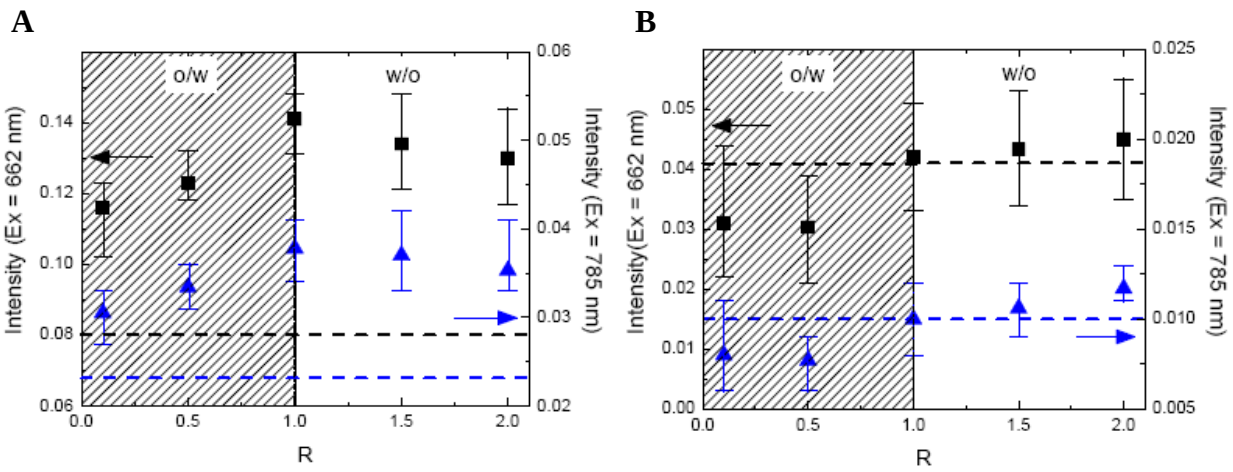

Figure 2-5. Fluorescence emission intensity fluctuations of the (7, 6) nanotube as a function of the volume ratio (R). The sample was prepared from an initial mass concentration of A) 0.03 or B) 0.005 mg/mL raw SWNTs. Excitation at 662 (■) and 784 nm (▲). Conductivity measurements suggests the formation of oil-in-water (o/w) emulsions (shaded area) for $R < 1$ and water-in-oil emulsions (w/o) for $R > 1$. The dashed lines represent the fluorescence spectra for the suspension after homogenization and ultrasonication

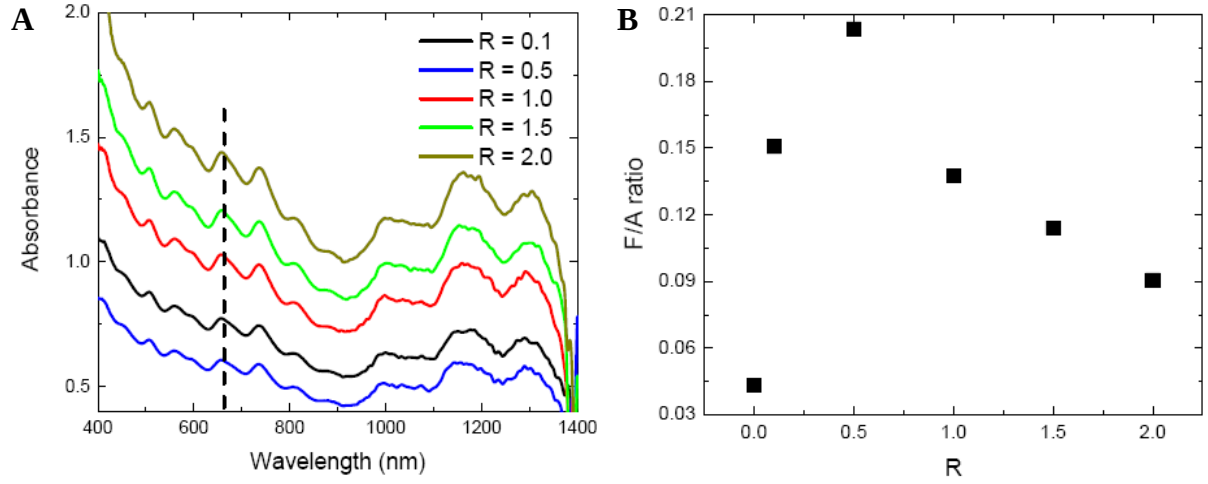

Figure 2-6. A) Absorbance spectra of Gum Arabic-suspended SWNTs and B) fluorescence to absorbance ratio fluctuations as a function of the volume ratio (R). The fluorescence intensity was measured for the (7, 6) nanotube and divided by the absorbance at the excitation wavelength (dashed line at 662 nm). The suspension was prepared from an initial concentration of 0.03 mg/mL raw SWNTs.

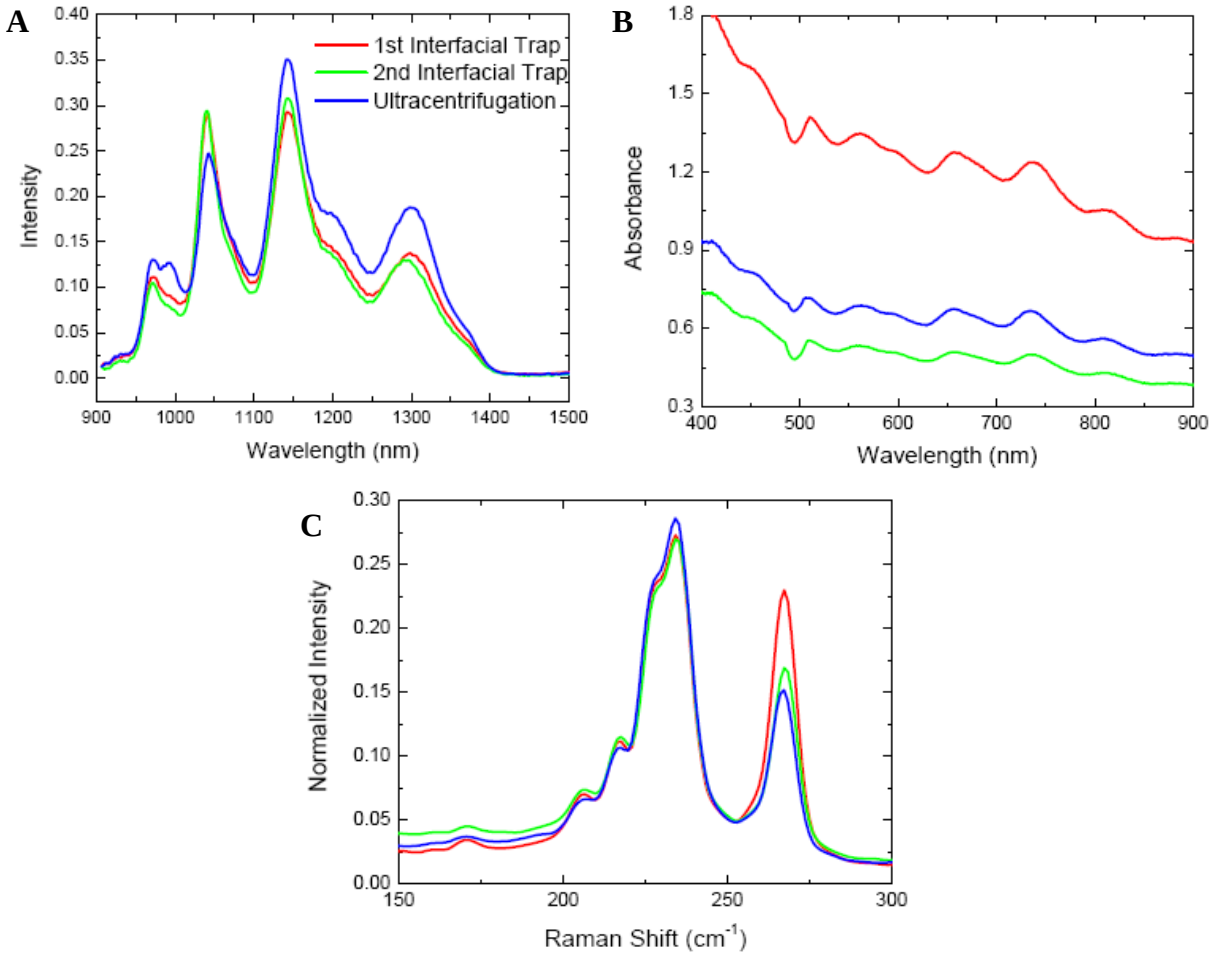

Figure 2-7. A) Fluorescence (ex = 662 nm), B) absorbance, and C) Raman RBM spectra (ex = 785 nm) of Gum Arabic-suspended SWNTs for one-step and two-step interfacial trapping separations compared to ultracentrifugation. The suspensions were prepared from an initial concentration of 0.2 mg/mL raw SWNTs.

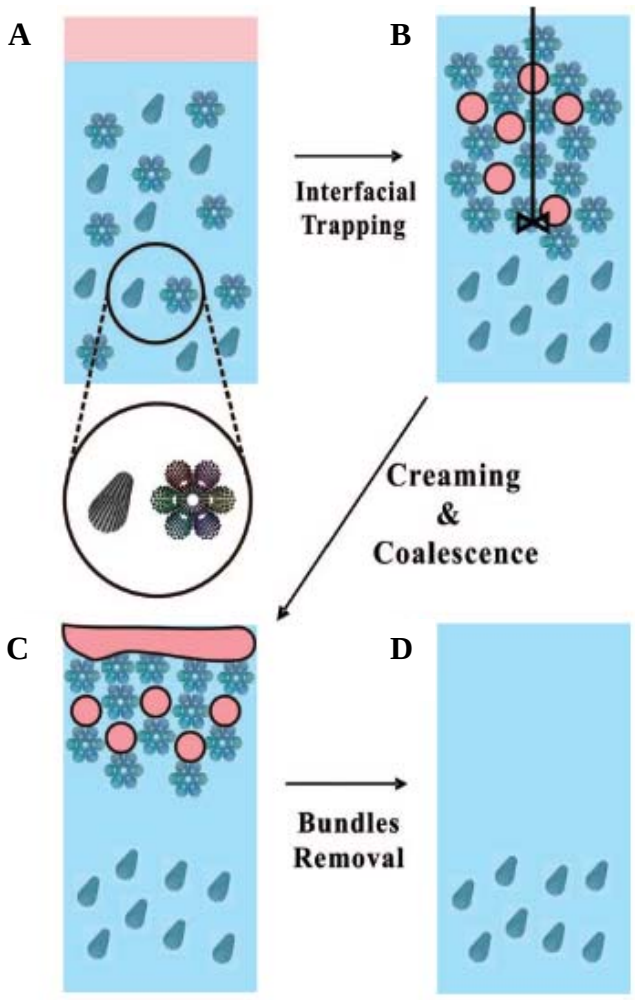

Figure 2-8. Overall process of removing SWNT bundles from aqueous suspensions via liquid–liquid interfaces. Prior to interfacial trapping, the raw SWNTs are first homogenized with a high- shear mixer and ultrasonicated to coat SWNTs with surfactant (not shown), resulting in a mixture of individually suspended SWNTs and SWNT bundles. A) Toluene is added to the aqueous phase and mixed to form emulsions, B) SWNT bundles are trapped at the emulsion interfaces, C) creaming and coalescence of emulsions separates the bundled SWNTs, and D) SWNT bundles are removed from the bulk aqueous fluid.

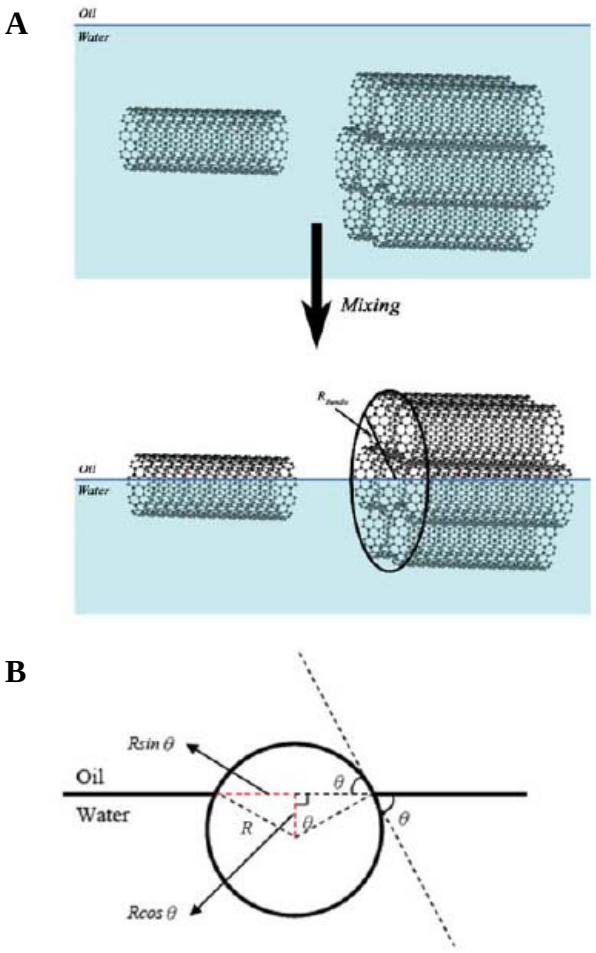

Figure 2-9. Adsorption process of an individual or bundle of nanotubes at the interface of the oil and water phases. A) Prior to interfacial trapping, individual or bundled nanotubes are dispersed in the aqueous phase. After mixing, the nanotubes assemble at the interface. B) Diagram showing the end of a nanotube at the interface where R is the radius of an individual or bundled nanotube and θ is the contact angle measured into the water phase.

Table 2-1. Dispersion Quality Comparison of Aqueous SWNT Suspensions.

	aqueous suspension			
anaylsis	control	interfacial trapping	ultracentrifugation	two-step interfacial trapping
fluorescence intensity	weak	strong	strong	strong
absorbance features	broad peaks	blue-shifted and resolved peaks	blue-shifted and resolved peaks	blue-shifted and resolved peaks
resonant Ratio[1]	0.0118	0.0397	0.0486	0.0406
diameter distribution[2]	12.8 ± 11.9 nm	4.1 ± 3.7 nm	—	—
Raman aggregation ratio[3]	0.7265	1.1868	1.8860	1.5952
F/*A* Ratio[4]	0.0135	0.2300	0.5234	0.6077

[1] Calculation based on peak near 660 nm.

[2] Distribution determined from AFM and SIMAGIS image analysis.

[3] Calculation based on intensity from (11, 3) nanotubes and aggregation peak (~270 cm^{-1}).

[4] Calculation based on fluorescence intensity from (7, 6) nanotubes and absorbance at 662 nm

CHAPTER 3
INTERFACIAL TRAPPING OF SWNT BUNDLES SUSPENDED WITH ANIONIC SURFACTANTS

Single-walled carbon nanotubes (SWNTs) are one of the most widely researched nanomaterials due to their unique physical and chemical properties. [4, 5] One of their unique properties is the emission of near-infrared (NIR) fluorescence, [2] which enables potential applications of SWNTs as optical devices for bioimaging [66, 67] and biosensing. [32, 68, 69] However, most applications require suspensions of individual SWNTs since bundled SWNTs can perturb the electronic structure of individual SWNTs, quenching their fluorescence, [2, 9, 10] or slip past one another under stress, weakening composite structures. [41]

SWNTs are typically dispersed in common solvents [36, 70] or in water with the aid of surfactants. [9, 15, 71] Ultrasonication is used to separate individual SWNTs from SWNT bundles; however, the strong van der Waals attractive forces [8] make it difficult to isolate all SWNTs without significant damage. [16] Therefore, SWNT bundles still remain in the suspension, which can be removed by high-speed ultracentrifugation because of density differences between bundled and individual SWNTs. [9] However, the small mass requires high centrifugal forces (> 100,000g) and long processing times to achieve separation (~ 4 to 5 h). These requirements limit the scalability of the process. Ultracentrifugation was the only route to remove the remaining bundles until our group recently developed a simple and novel interfacial trapping (IT) process to remove SWNT bundles. [34, 72] High yields of aqueous SWNT suspensions were prepared using the nonionic surfactant gum Arabic. These SWNT suspensions were also comparable in dispersion quality to those prepared by ultracentrifugation. [72] Li and co-workers have used the IT process in fabricating field effect transistor (FET) devices. The IT-based FET devices showed at least an order of magnitude improvement in on/off ratios compared to those devices prepared by ultracentrifugation only. [42]

The IT process for preparing aqueous SWNT suspensions is based on selective partitioning of SWNT bundles to liquid-liquid interfaces. The liquid-liquid system is mixed to form emulsions and increase interfacial area. As the SWNT bundles move to the interface, they help stabilize emulsions, known as Pickering emulsions, [21] which aid the separation. The driving force for the selective removal of SWNT bundles is the free energy changes associated with particles adsorbing at interfaces. [64, 72] Bundled SWNTs have larger radii and lengths, thereby taking up larger interfacial area than individual SWNTs. [72] However, the properties of the SWNT surface also play an important role, which is reflected in the surface tension of the nanotubes or contact angle (θ) of the system. The interfacial activity of particles (or emulsion stability) is related to the hydrophobicity/hydrophilicity of the particles with $\theta = 90°$ yielding the strongest driving force for particles at interfaces. [26] In other words, highly hydrophobic or hydrophilic surfaces will not self-assemble at interfaces. This poses problems for separating SWNT bundles coated with ionic surfactants. Anionic surfactants, such as sodium dodecyl sulfate (SDS), sodium dodecylbenzene sulfonate (SDBS), and sodium cholate (SC), are preferred in SWNT applications [15, 71] because of the strong electrostatic repulsion, [73] yielding suspensions with high fluorescence intensity.

In this chapter, we demonstrate that bundled SWNTs coated with the anionic surfactant, sodium cholate (SC), can be removed from aqueous suspensions by IT. The dispersion quality of SC-suspended SWNT suspensions were improved by adjusting the initial pH of the suspension so that the surface charge on the SWNT-surfactant complex was a minimum. A two-step interfacial trapping process further improved the dispersion quality, providing final suspensions comparable to those produced by ultracentrifugation.

3.1 Experimental Procedure

3.1.1 Dispersion and Interfacial Trapping

SWNT suspensions were prepared with a given initial mass (~ 8 mg) of raw SWNTs (Rice HPR 177.1) and mixed with 50 mL of an aqueous SC (Sigma-Aldrich) surfactant solution (1 wt.%) to form an initial concentration of ~ 0.16 mg/mL. To aid dispersion, the solutions were homogenized using a high-shear IKA T-25 Ultra-Turrax mixer for about 1 – 1.5 h followed by ultrasonication using a Misonix S3000 for 10 min. A portion of the initial SWNT suspension was then ultracentrifuged at 20,000 rpm (Beckman Coulter Optima L-80 K) for 5 h. The supernatant was carefully collected to remove the aggregated nanotubes. [9] The remaining portion of the SWNT suspension was added to toluene (Acros, 99%) at an oil to water volume ratio of 0.1 to form a two-phase system. In some cases, the pH of the aqueous suspension was adjusted by adding 1 M hydrogen chloride (HCl). The two-phase system was then shaken vigorously by a vortex mixer for 30 s. Phase separation started immediately but the suspensions were allowed to settle for 60 min to ensure steady state for spectroscopic analysis. The organic layer was then carefully removed to avoid further emulsification.

3.1.2 Characterization

Vis-NIR absorbance and NIR-fluorescence spectra were measured for each aqueous SWNT suspension using an Applied NanoFluorescence Nanospectrolyzer (Houston, TX) with excitation from 662 and 784 nm diode lasers. Raman Spectra were recorded by a Reinshaw Invia Bio Raman with excitation at 785 nm. The zeta-potentials of the SWNT-surfactant complex were recorded at different pH with a Brookhaven ZetaPlus.

3.2 Results and Discussion

3.2.1 Selective Separation of Bundles

Measuring the dispersion quality of SWNT suspensions remains challenging. Spectroscopic techniques, including absorbance, fluorescence, and Raman, are typically the best approaches [14] and were shown to be effective in evaluating the IT process based on gum Arabic (GA) suspensions. [72] Figure 3-1 shows spectroscopic analysis for the initial (homogenized and sonicated), ultracentrifuged, and IT SWNT suspensions. The Raman spectra (Fig. 3-1 (A)) show the initial suspension (curve 1) has a significant aggregation peak, measured at ~270 cm^{-1}, as expected for a suspension that still has a significant fraction of bundled SWNTs. The absorbance of the initial suspension is also high (not shown). Although the fluorescence intensity of the initial SWNT suspension is relatively high (Fig. 3-1 (C)), it is clear that the dispersion quality is low once the ratio of the fluorescence intensity to absorbance (F/A) is calculated (Fig. 3-1 (D)). [72] The ultracentrifuged SWNT suspension (curve 2) shows significant improvement in dispersion quality with a reduced aggregation peak (Fig. 3-1 (A)), low background absorbance (Fig. 3-1 (B)), and high F/A ratio (Fig. 3-1 (D)).

Multi-step IT was previously shown to be effective at achieving high dispersion quality of SWNTs suspended with GA. [72] Similarly, the first IT process (one-step, curve 3) on SC-SWNT suspensions showed improvement to the aggregation peak (Fig. 3-1 (A)) and absorbance (Fig. 3-1 (B)). The fluorescence intensity increased after the one-step IT (Fig. 3-1 (C)), similar to the previous observations with GA-suspended SWNTs. [72] This increase in intensity is attributed to a reduction in quenching once bundles are removed from the suspension. Despite the high fluorescence intensity, the dispersion quality remains lower than the ultracentrifuged SWNT suspensions (Fig. 3-1 (D)). Repeated IT steps (curves 4 – 5) continued to improve the dispersion quality, as seen by a lower aggregation peak and lower background absorbance. The

significant decrease in background absorbance coupled with the relatively constant fluorescence intensity suggests that the IT process is selective in removing bundled SWNTs from the aqueous suspension, as previously observed. [72] However, even after three consecutive IT steps, the suspension remains lower in dispersion quality than those suspensions prepared by ultracentrifugation. This indicates that the IT process is inefficient at these conditions.

3.2.2 Improving Separation Effectiveness

The charge on the SWNT-surfactant complex was adjusted to improve the efficiency of the IT separation process. Figure 3-2 (A) shows the zeta potential of the SWNTs in a SC suspension as a function of pH. The zeta potential of the SWNTs shows a strong pH dependency. The initial suspension (pH = 7.9) has a large negative charge on the SWNTs in agreement with other reports. [74, 75] As the pH is adjusted to more acidic conditions, the charge on the SWNTs goes through a sharp minimum centered at pH = 6.75. The pH-adjusted aqueous SWNT suspensions were then mixed with toluene using the one-step IT process. Figure 3-2 (B) shows the F/A ratio for each SWNT suspension after IT. It is clear that pH (surface charge) on the SWNTs has an important effect on the separation efficiency in the IT process. The most significant differences are observed for the smallest diameter SWNTs (lower emission wavelength) where different pH could yield F/A ratios that could vary by a factor of two. The fluorescence spectra was deconvoluted into the individual (n, m) SWNT types. The normalized intensity of each (n, m) type was then plotted as a function of pH, as shown in Figure 3-2 (C) for the (6, 5), (8, 3), and (10, 5) SWNT types. It is clear that the efficiency of the IT process is highly correlated to the surface charge on the SWNTs. The suspensions with the best dispersion quality (highest F/A ratio) were obtained when the zeta potential was at a minimum.

The dependence of dispersion quality or SWNT bundle removal efficiency on surface charge was confirmed through Raman spectroscopy, as shown in Figure 3-2 (D). The

aggregation ratio of the SWNT suspension (ratio of the intensity of (11, 3) SWNT to the aggregation peak) is presented in Figure 3-2 (E) as a function of pH. Once again, the best aggregation ratios match the minimum zeta-potential value at pH 6.75, which indicates the best dispersion quality in agreement with *F*/*A* ratio measurements.

Prior studies have shown that mixing organic solvents with aqueous suspensions can alter the surfactant structure surrounding SWNTs. [76] This reorganization of surfactant can improve the fluorescence intensity by eliminating quenching mechanisms. Before further comparisons are made between the pH-adjusted IT process and ultracentrifugation, solvent-induced changes to the spectra must be addressed. The ultracentrifuged SC-SWNT suspension was mixed with toluene and then evaporated for 24 h similar to the IT processing steps. Figure 3-3 shows the fluorescence spectra of ultracentrifuged SC-SWNTs at each stage of the process. The consistent spectra throughout the process show the solvent has minimal influence on the surfactant structure or the fluorescence intensity. The lack of spectral changes could be due to the strong interaction that SC has to the sidewall of the SWNTs. [77] Therefore, any changes to the spectra observed during IT can be attributed to the removal of bundled SWNTs.

Figure 3-4 compares the spectral properties of SWNTs prepared by either the pH-adjusted two-step interfacial trapping process (pH 6.75) or ultracentrifugation. The *F*/*A* ratio in Figure 3-4 (A) and 3-4 (B) show that SC-SWNT suspensions prepared by IT can achieve comparable dispersion quality to ultracentrifugation SWNT suspensions. The Raman spectra in Figure 3-4 (C) also show similar dispersion quality. However, the absorption spectra in Figure 4d show the concentration of individual SC-SWNTs in suspensions made by IT is almost double the concentration achieved by ultracentrifugation. This indicates that the two-step IT process has twice the yield of SWNTs in comparison to ultracentrifugation. To further illustrate the higher

throughput, the IT suspension was diluted with 1 wt.% SC until the absorbance was nearly the same as the ultracentrifuged SWNT suspension. As can be seen in Figures 3-4 (A) – 3-4 (D), the dilution has little effect on the dispersion quality. This dilution may also have added benefit to dispersion stability by adjusting the surface charge (pH) to higher values (see Fig. 3-2).

Table 3-1 summarizes the dispersion quality measurements for the two-step IT process (pH adjusted) compared to ultracentrifugation. The table shows that the IT process has similar dispersion quality to ultracentrifugation, as measured by multiple characterization methods. Table 3-2 summarizes the processing parameters and results for the two-step IT and ultracentrifugation approaches to preparing SC-SWNT suspensions. As seen in the table, the IT process has favorable processing times, yields, and throughput. These characteristics and the simplicity of the process enable a fast and scalable approach to preparing SWNT suspensions with good dispersion quality. In addition, the IT process is more conducive to parallel processing, which will further improve throughput.

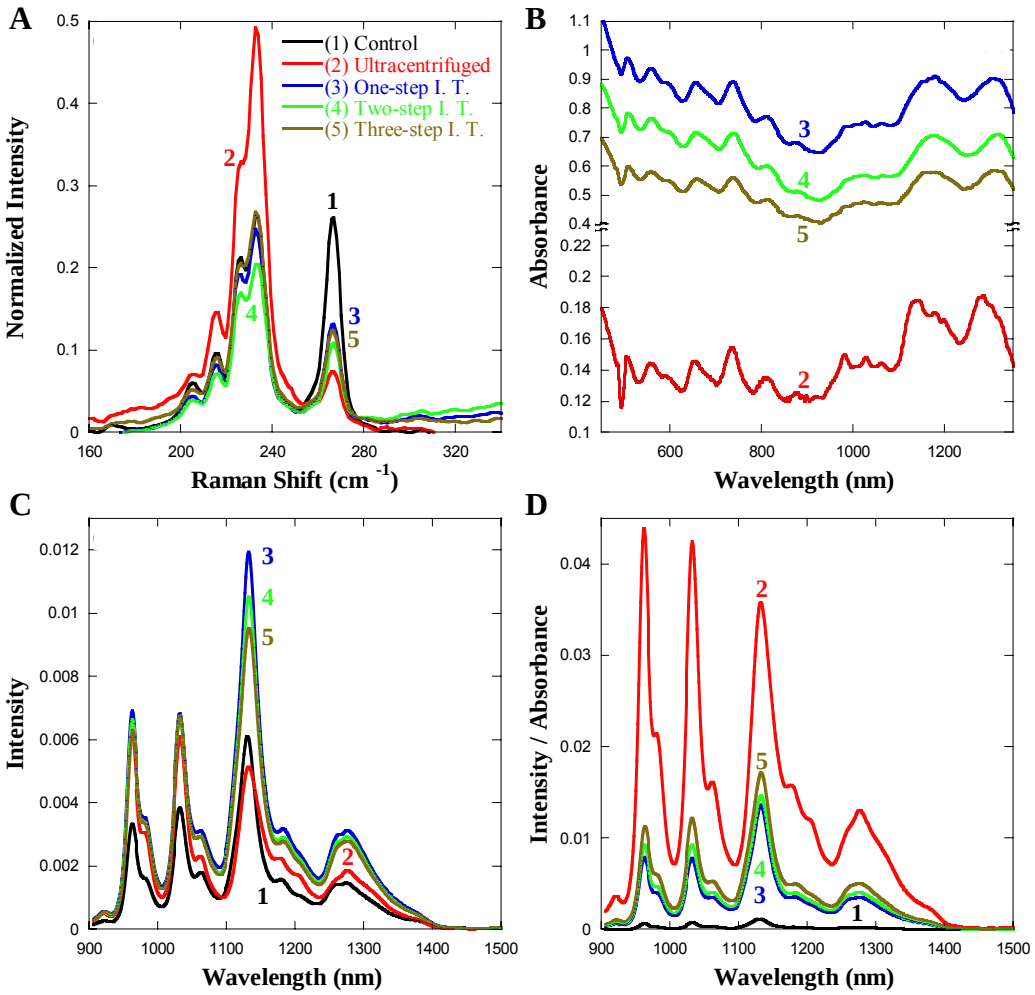

Figure 3-1. A) Radial breathing mode (RBM) of Raman spectra, B) Vis-NIR absorption spectra, C) NIR-fluorescence spectra (662 nm excitation), and D) Fluorescence / absorbance ratio (calculated from 662 nm) of SC-suspended SWNTs. (1), (2), (3), (4) and (5) represent the control, ultracentrifuged, one-step interfacial trapped, two-step interfacial trapped, and three-step interfacial trapped SC-SWNTs, respectively.

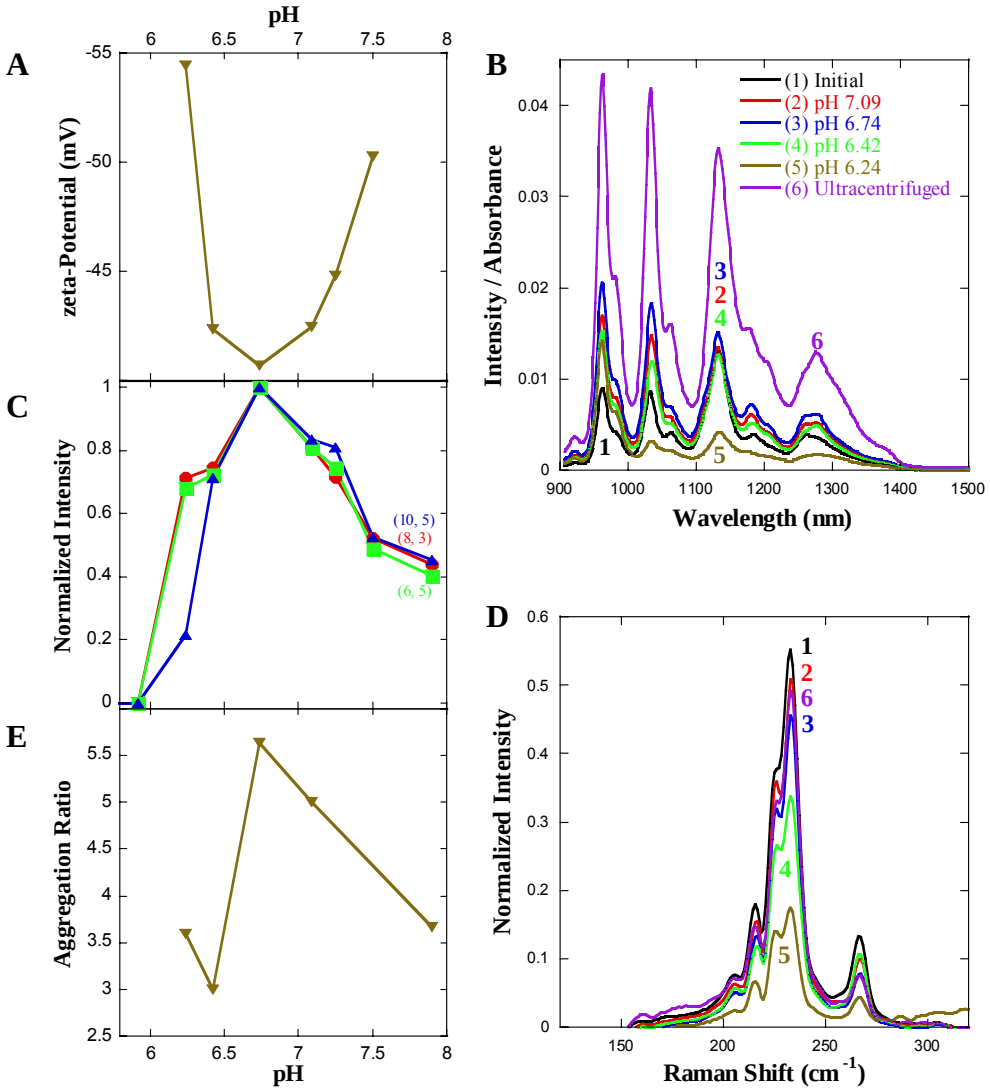

Figure 3-2. A) The pH-dependent changes to the zeta-potential of SC-SWNTs. B) The effect of pH on the intensity/absorbance ratio after interfacial trapping. The surface charge was adjusted by changing the pH of the suspensions prior to IT. C) The effect of surface charge on the intensity of (6,5), (8,3), and (10,5) SWNT types after interfacial trapping. All intensities are normalized to the maximum intensity. D) pH-dependent Raman spectra (784 nm excitation) of the radial breathing modes (RBMs) of SWNTs. Spectra are normalized to the G band. E) The effect of surface charge on the Raman aggregation ratio.

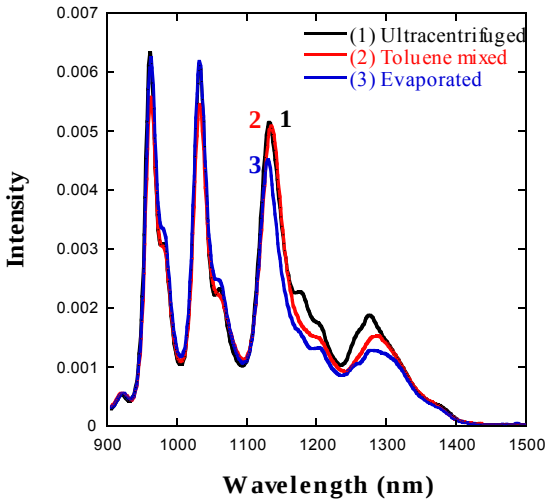

Figure 3-3. The effect of solvent on the fluorescence intensity of ultracentrifuged SC-SWNTs (662 nm excitation). The ultracentrifuged SWNTs (1) are first mixed with toluene (2). The toluene was then removed by evaporation (3).

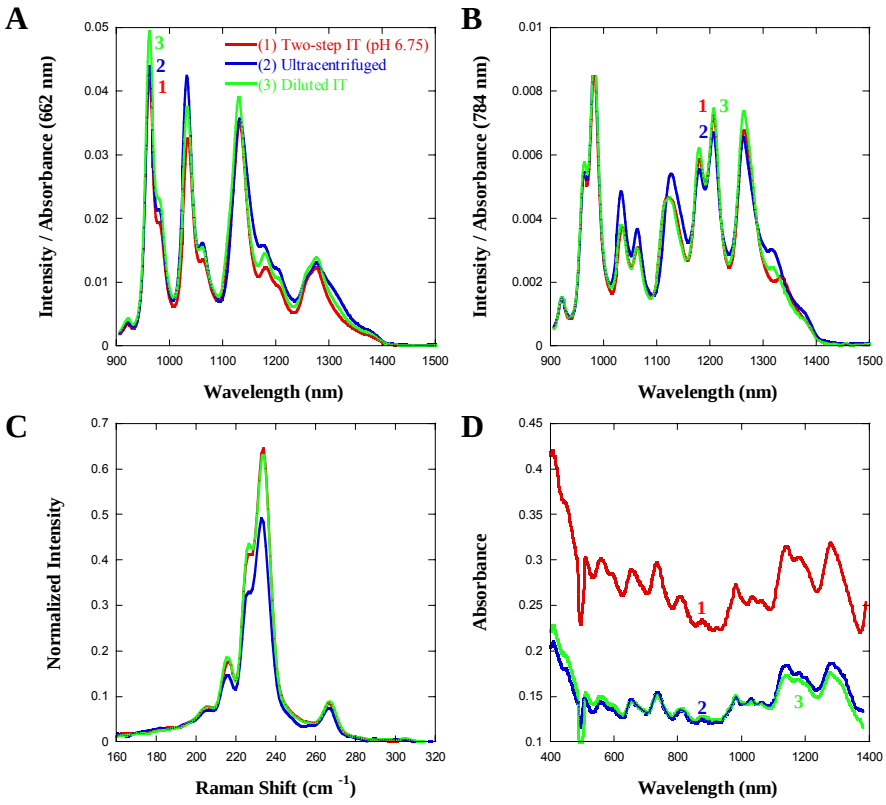

Figure 3-4. Comparison of SC-SWNT suspensions prepared by the pH-adjusted (pH 6.75) two-step IT process (1), ultracentrifugation (2), and dilution of the IT process (3) obtained from (1). The ratio of fluorescence intensity to absorbance for SWNT suspensions excited at A) 662 and B) 784 nm. C) Raman spectra of the SWNT RBMs. D) Absorption spectra of the suspensions.

Table 3-1. Dispersion Quality Comparison of Aqueous SWNT Suspensions.

	aqueous suspension		
anaylsis	control	ultracentrifugation	two-step interfacial trapping
fluorescence intensity	weak	strong	strong
absorbance features	broad peaks	blue-shifted and resolved peaks	blue-shifted and resolved peaks
resonant ratio[1]	0.015	0.070	0.057
Raman aggregation ratio[2]	1.00	6.25	7.22
F/*A* Ratio[3]	0.0014	0.0358	0.0352

[1] Calculation based on ratio of resonant and nonresonant features of the absorbance peak near 660 nm.

[2] Calculation based on intensity from (11, 3) nanotubes and aggregation peak (~270 cm^{-1}).

[3] Calculation based on fluorescence intensity from (7, 6) nanotubes and absorbance at 662 nm.

Table 3-2. Comparison of the processing parameters for the pH-adjusted two-step interfacial trapping (pH 6.75) and ultracentrifugation methods for producing high quality SWNT suspensions.

Method	Processing Time	SWNT Yield	Throughput (per liter)
Interfacial Trapping	< 2 h	Large (4~24%)	3 ~ 10 mg/h
Ultracentrifugation	> 5 h	Small (< 2%)	< 1 mg/h

CHAPTER 4
SWELLING THE MICELLE CORE SURROUNDING SWNTS WITH WATER-IMMISCIBLE ORGANIC SOLVENTS

Single-walled carbon nanotubes (SWNTs) are tubular structures of carbon with several unique physical and chemical properties. [4, 5] Dispersing SWNTs in a solvent is required for many applications but common organic solvents offer insufficient solvation forces to suspend SWNTs. [36] Surfactants or polymers are often used to stabilize aqueous SWNT suspensions. The hydrophobic part of the surfactant non-covalently attaches to the sidewall of the nanotubes while the hydrophilic end extends into the water phase. The resulting surfactant shell creates a repulsive barrier that overcomes the strong van der Waals attractive forces needed to disperse the SWNTs. [8] The anionic surfactants sodium dodecyl sulfate (SDS) and sodium dodecylbenzene sulfonate (SDBS) are frequently used because of the high dispersion quality of the resulting SWNT suspensions.

The ability to individually disperse SWNTs in solution enabled the discovery of NIR fluorescence of semiconducting nanotubes, [9] which correspond to the specific (n, m) type of each nanotube as mentioned in previous paragraph. The fluorescence emission energies of SWNTs are sensitive to the surrounding environment with suspended SWNTs being red-shifted in comparison to SWNTs in air. [78-80] The extent of the energy shift is dependent on the surfactant, [15] protein, [66, 67, 81, 82] or polymer that encases the nanotube. [83, 84] The first measurements of the photoluminescence quantum yields for dispersed SWNTs were on the order of 0.1% or less. [9, 10] The optically excited electronic states of SWNTs are highly mobile, [85] making them sensitive to extrinsic effects that can reduce the quantum yield, including sidewall defects, [57, 80, 85-87] protonation, [85, 88-90] surfactant inhomogeneties, [57, 86, 87, 91] bundles, [57-59, 92] and nanotube ends (i.e., lengths). [93, 94] Indeed, single-molecule spectroscopy in both aqueous solutions [86] and air [80] have observed spots along the length of

a nanotube, which have reduced fluorescence emission intensity. These dark spots allowed Cognet et al. [85] to estimate the exciton diffusion length to be ~90 nm. When the quantum yields are calculated on single nanotubes that have no dark spots, the quantum yields improve dramatically to values approaching 10%.[80, 85, 86]

The observation of these extrinsic factors has raised questions regarding the capability of fluorescence spectroscopy to quantify relative (*n*, *m*) ratios. [80, 86] The difference in quantum yield measurements seen for bulk-scale suspensions and single-molecule analysis points to the importance in understanding how SWNT dispersion affects fluorescence intensities. For example, different quantum yields are observed for different surfactants. [91] Differences in fluorescence intensity between different surfactant suspensions also led to the conclusion that some surfactants, such as SDS, preferably disperse small diameter SWNTs. [78] The ultimate objective is to learn how to compensate for these differences. [86] Recently, the elimination of small bundles was shown to improve the quantum yields of bulk SWNT suspensions to ~1 – 1.5%. [92]

Understanding the importance of these extrinsic factors to the quantum yields of SWNTs may be compounded by an incomplete understanding of the surfactant structure surrounding the nanotube. In general, three models of surfactant structure have been suggested: (a) hemisphere, [17] (b) cylindrical, [95] and (c) randomly adsorbed surfactant structures surrounding the nanotubes. [18] However, there is no accepted structure for the surfactant surrounding the nanotubes. Wallace et al. [20] showed through coarse-grained molecular dynamics (MD) calculations that the surfactant structure around SWNTs was concentration dependent. At low concentrations, the surfactant molecules tend to orient themselves along the length of the nanotube. However, the surfactant extends out into the aqueous phase at higher concentrations.

These simulations combined with the previously observed extrinsic factors suggest that processing conditions may play an important role in the photophysical properties of SWNT suspensions.

In this chapter, we describe the swelling of the hydrophobic core of the micelle surrounding the SWNTs. Mixing aqueous suspensions of SWNTs with various immiscible organic solvents results in solvatochromic shifts indicative of a coating surrounding the nanotubes. The solvatochromic shifts and changes in the fluorescence intensity are dependent on the surfactant coating the nanotube, allowing the spectral changes to be used to probe the surfactant structure around SWNTs. While the solvatochromic shifts are reversible once the solvent is removed, the fluorescence intensity depends on the surfactant-solvent combination used to swell the micelle. For SDS-coated SWNTs, the largest diameter nanotubes show significant increases in fluorescence intensity after some organic solvents are removed. In addition, these SWNTs are better protected from the fluorescence quenching effect of acid. The spectral changes suggest that the organic solvent is capable of reorganizing the surfactant surrounding the SWNT.

4.1 Experimental Procedure

4.1.1 Dispersion

SWNT suspensions (Rice HPR 145.1) were prepared in both 1 wt% SDS and SDBS solutions followed by ultracentrifugation. Aqueous nanotube suspensions were prepared by mixing 20 mg of raw SWNTs with 200 mL of an aqueous SDS or SDBS surfactant solution (1 wt. %). High-shear homogenization (IKA T-25 Ultra-Turrax) for 1.5 – 2.0 h and ultrasonication (Misonix S3000) for 10 min were used to aid dispersion. After ultrasonication, the mixture was ultracentrifuged at 20,000 rpm for 5 h (Beckman Coulter Optima L-80 K). Immiscible solvents, such as o-dichlorobenzene (ODCB), were added to each SWNT suspension (solvent: water

volume ratio of 0.5) and mixed. The mixture was shaken vigorously for 30 s with a vortex stirrer. After shaking, a white emulsion phase immediately started to phase separate. The characterization of aqueous SWNT suspensions was done after waiting for 1.5 - 2 h to reach steady state. The excess organic solvent was then carefully removed from the aqueous SWNT suspension to prevent further emulsification. SWNT suspensions prepared in pure ODCB were ultrasonicated and then filtered through coarse filter paper to remove the large visible aggregates in the suspension prior to characterization. [9]

4.1.2 Characterization

The aqueous phase was characterized by vis-NIR absorbance and NIR-fluorescence spectra using an Applied NanoFluorescence Nanospectrolyzer (Houston, TX) with excitation from 662 and 784 nm diode lasers. Raman spectra were recorded with a Renishaw Invia Bio Raman with excitation from a 785 nm diode laser.

4.2 Results

Figure 4-1 shows the NIR fluorescence spectra for the initial aqueous SWNT suspension and the aqueous suspension after mixing with ODCB. In both the SDBS- and SDS-SWNT suspensions, the peaks have red-shifted by 0.01 – 0.1 eV (9 – 17 nm) indicating a change to the environment surrounding the nanotubes. The fluorescence intensity has also significantly decreased in both suspensions. In SDS suspensions, the fluorescence emission from the largest diameter SWNTs has almost completely disappeared.

Nanotubes have limited solubility in pure ODCB without using surfactants, [36] allowing direct comparison to aqueous suspensions mixed with ODCB. Figure 4-2 compares the normalized fluorescence spectra of ODCB-suspended nanotubes to aqueous SDS- and SDBS-suspended nanotubes after mixing with ODCB. Once the SDBS- and SDS-coated aqueous SWNT suspensions are mixed with ODCB, the suspensions show similar emission spectra to

SWNTs dispersed in pure ODCB. The smallest diameter nanotubes (larger emission energy) have very good agreement in peak position with nanotubes in ODCB, especially for SDBS-coated SWNTs. The similarity in the spectra implies that ODCB molecules are in close proximity to the nanotubes.

The organic solvent was removed from the surfactant-coated SWNT suspensions by room temperature evaporation for 24 h. Figure 4-3 (A) shows the fluorescence spectra for SDS-coated SWNT suspensions during evaporation of ODCB. The time dependent changes to the intensity of the (7, 6) and (8, 3) nanotubes are shown in Figure 4-3 (B). The smallest diameter nanotubes (e.g., (8, 3) SWNTs) recover their fluorescence intensity faster than the larger diameter nanotubes (e.g., (7, 6) SWNTs). All nanotube fluorescence intensities have reached equilibrium after ~20 h. The spectra for both SDS- and SDBS-suspended SWNTs return to their original peak positions and have intensities close to their initial values (compare Fig. 4-1 (B) for SDS-suspended SWNTs, discussed further below).

Spectral changes were also observed for aqueous SWNT suspensions mixed with other organic solvents. Figure 4-4 plots the fluorescence spectra of SDBS- and SDS-suspended SWNTs mixed with various organic solvents. Once again, the solvatochromic shifts and changes to fluorescence emission intensity were dependent on the surfactant used to suspend the SWNTs. For each solvent, the SDBS-suspended SWNTs in Figures 4-4 (A) and 4-4 (C) showed similar changes to both the solvatochromic shifts and fluorescence intensity for each (n, m) SWNT type. SDBS-SWNT mixtures with hexane showed a slight increase in fluorescence emission and blue-shifts. On the other hand, mixtures of benzene with SDBS-SWNTs showed red-shifts and both slight increases and decreases in fluorescence intensity. Finally, chloroform mixtures with SDBS-coated SWNTs had similar decreases in intensity and red-shifts as the ODCB mixtures. In

contrast to the SDBS-coated SWNT suspensions, the SDS-SWNTs in Figures 4-4 (B) and 4-4 (D) showed changes to the fluorescence intensity, which was dependent on the SWNT (*n*, *m*) type. The emission spectra for SDS-SWNTs red-shift and significantly decrease in intensity for hexane mixtures while benzene mixtures have small blue-shifts of the emission and significant increases in fluorescence intensity. The response of SDS-SWNTs mixed with chloroform was diameter dependent and varied slightly between different suspensions. In general, the small diameter nanotubes (e.g., (8, 3) SWNTs) have minor changes to both emission energy and intensity while large diameter nanotubes show no shifts but large decreases in intensity. Similar to mixtures with ODCB, the intensity of the largest diameters (e.g., (9, 5) SWNTs) almost completely disappeared.

Table 4-1 summarizes the fluorescence emission of SWNT suspensions after being mixed with each solvent. In general, all systems that red-shift show decreases in fluorescence intensity. Figure 4-4 also shows that the largest diameter SWNTs have the most significant decreases in fluorescence emission intensity. The spectral shifts for SDBS-coated SWNTs closely mirror the differences in dielectric constant and polarity of the organic solvent. However, there is no apparent trend of the spectral changes of the SDS-coated SWNT suspensions with the solvent. The largest decreases in fluorescence intensity occurred when mixed with the solvent that has the highest dielectric constant (ODCB) and the lowest dielectric constant (hexane). The polarity also seems to have no influence on the fluorescence intensity since the two non-polar species showed the ability to either decrease (hexane) or increase (benzene) the intensity after mixing with the aqueous SWNT suspensions.

The spectra for both SDBS- and SDS-suspended SWNTs exposed to immiscible solvents return to their original peak positions after the solvent is evaporated from the aqueous suspension

and have intensities close to the surfactant only SWNT suspensions, as shown in Figure 4-5. This is somewhat surprising for SDS-suspended nanotubes since the peaks had nearly disappeared in Figures 4-4 (B) and 4-4 (D) after mixing with ODCB, chloroform, and hexane. For example, the fluorescence spectra for SWNTs mixed with ODCB in Figures 4-4 (B) and 4-4 (D) shows the fluorescence of only the (8, 3), (7, 5) and (6, 5) SWNT types. After the evaporation of ODCB, the fluorescence emission from all SWNT (*n*, *m*) types return, as shown in Figures 4-5 (B) and 4-5 (D). There are some minor differences in the intensity of SDBS-coated SWNTs after exposure to the organic solvents, which may be attributed to removal of nanotubes or impurities at the interface. [34, 72] On the other hand, substantial increases to the fluorescence intensity for SDS-suspended SWNTs are observed after ODCB and chloroform have evaporated. For example, the large diameter SWNTs in Figures 4-5 (B) and 4-5 (D) have considerable increases in fluorescence emission intensity after the organic solvent is removed.

These changes in fluorescence intensity occur without any differences to the relative ratios between (*n*, *m*) types in either the absorbance or Raman spectra. The absorbance spectra after the solvent is removed from the aqueous suspension in Figure 4-6 (A) show that, in general, the spectra are similar to the initial SWNT suspension. Although the SDS-SWNT suspensions exposed to ODCB and chloroform have minor changes to the absorbance baseline, there are no changes to the ratio of peak heights. The decrease in absorbance observed with chloroform would indicate further proof that impurities were removed from the system. [34, 72] Most importantly, there is no broadening or red-shifting of the peaks for any of the spectra. The radial breathing modes (RBMs) of the Raman spectra are dependent on the diameter of the nanotubes and can also indicate changes to the (*n*, *m*) types. As seen in Figure 4-6 (B), the intensity of the Raman RBMs for each peak is nearly identical to that observed for the initial SDS-SWNT

suspension. Note that the (10, 5) SWNT has the largest intensity increase in Figure 4-5d. In addition, there are no changes to the so-called aggregation peak (~270 cm^{-1}) after the organic solvents are removed. These results indicate that the suspension has no significant changes to the relative concentration of nanotube (*n*, *m*) types or bundling, which could cause the changes in fluorescence emission seen in Figures 4-5 (B) and 4-5 (D). [34, 59, 86, 91, 96]

4.3 Discussion

4.3.1 Swelling Effects

The solvatochromic shift in fluorescence emission spectra of SWNTs mixed with organic solvents indicates a change to the environment surrounding the nanotubes. When compared to SWNTs suspended in pure organic solvents, these spectra show nearly identical peak positions (see Figure 4-2) suggesting that organic solvents are forming a layer or a shell around the sidewall. Since the fluorescence, absorbance, and Raman spectra return to the initial values after the solvent has evaporated, the surfactant must still be present. Otherwise, there would be substantial bundling of the nanotubes resulting in broadened and red-shifted absorbance as well as quenching of the fluorescence emission. [9, 86, 91] The reversibility of both the spectral shifts and intensities is good evidence that the presence of the organic solvent molecules rather than aggregation or surfactant removal is responsible for the observed changes. Therefore, the data suggests that the organic solvent is swelling the hydrophobic region of the surfactant micelle surrounding the SWNTs, similar to the swelling of micelle cores in block copolymers, [97] as shown in Figure 4-7 (A). This conclusion is also supported by the consistent trend of the solvatochromic shift of SDBS-coated SWNT suspensions with solvent polarity (see Figures 4-4 (A), 4-4 (C) and Table 4-1), indicating that the environment around the nanotubes is systematically changing when mixed with different solvents.

The spectral changes observed for SDS-coated SWNT suspensions when mixed with organic solvents are more complex. In hexane mixtures, the fluorescence intensity of SWNTs increases significantly in Figures 4-4 (B) and 4-4 (D). On the other hand, fluorescence emission decreases considerably for other solvents. The presence of the organic solvents can affect the fluorescence intensity; [98] however, the solvatochromic shifts and intensity changes should tend to follow polarity changes as observed with SDBS-SWNT suspensions. The effect of each solvent should also yield consistent changes to the SWNT emission spectra. In other words, if a solvent (e.g, ODCB) is inducing changes to the emission spectra in Figures 4-4 (B) and 4-4 (D), similar changes to the emission spectra should be observed in the spectra in Figures 4a and 4c. The lack of a consistent trend for SDS-coated SWNTs (see Figure 4-4 (B), 4-4 (D) and Table 4-1) and the different response for each surfactant suggests that another phenomenon is responsible for the changes in SDS-coated SWNT suspensions.

Researchers have observed increased fluorescence intensity due to Förster energy transfer between individual SWNTs. [57-59, 79] For example, the emission of large diameter SWNTs (smaller band gap energy) was enhanced during nanotube bundling by excitation and energy transfer from the larger band gap, smaller diameter SWNTs. [58] If energy transfer is responsible for the increased fluorescence emission of large diameter SWNTs after solvent evaporation, then a decrease in fluorescence intensity would be expected for the smaller diameter SWNTs. However, the increases in nanotube emission intensity observed after chloroform and ODCB exposure occur without a simultaneous decrease in intensity from other SWNTs. The lack of any significant changes to the Raman aggregation peak also seems to rule out Förster energy transfer as the cause for increased fluorescence emission of some (n, m) types. The fact that a new peak corresponding to the (9, 7) SWNT appears in the emission spectra in Figure 4-5 (D) strongly

suggests that this species is present in the initial suspension but is not fluorescing. This behavior often is indicative of exciton energy transfer [57-59, 79] but this SWNT type is already observed in the spectra for SDBS-suspended SWNTs in Figure 4-5 (C) and the Raman spectra in Figure 4-6 (B). In fact, the spectra in Figures 4-5 (B) and 4-5 (D) after exposure to chloroform are strikingly similar in shape and relative intensity when compared to all of the spectra in Figures 4-5 (A) and 4-5 (C).

SWNTs are also susceptible to doping when the solvent is in close proximity to the surface. If solvent doping were responsible for the observed intensity changes after evaporation, then both SDS- and SDBS-coated SWNTs should have similar changes. As shown in Figure 4-1, both systems have a solvatochromic shift that indicates that ODCB is surrounding the SWNTs. However, only the SDS-SWNT suspensions show improvements to the fluorescence intensity in Figure 4-5. In addition, the nanotube (*n*, *m*) types which show decreases in intensity when the solvent is present are the same nanotube types that have increased emission after exposure to the solvents. For example, the fluorescence emission from the (7, 6), (12, 1), (11, 3), and (10, 5) SDS-SWNT suspensions in Figures 4-4 (B) and 4-4 (D) are completely quenched but then show the largest increases in intensity after evaporation in Figures 4-5 (B) and 4-5 (D). Without changes to the chemical structure of the solvent during evaporation, it is unlikely that solvent doping can cause this behavior. Recently, researchers showed that decomposition products of ODCB generated during ultrasonication could dope SWNTs. [99] However, the authors observed that mixing with solvents, similar to the approach in this study, does not cause decomposition or doping. To determine if photochemistry could initiate ODCB decomposition and doping during evaporation, SWNTs were also processed under natural light and dark conditions. The fluorescence spectra of the light and dark suspensions were identical (not shown) eliminating

decomposition-induced changes. Finally, Raman spectra after solvent evaporation show the G′ and G band do not have any shifts or width changes associated with doping. [99, 100] The G′ band in Figure 4-6 (C) is partially obscured by the background fluorescence but clearly shows that there are no shifts after solvent evaporation. [99, 100] Similarly, the G band in Figure 4-6d has no major changes to the shifts or width after evaporation. It does appear that ODCB may have a slight red-shift (~1 cm^{-1}); however, this would indicate a small amount of n-type doping rather than p-type doping observed previously. [99] The lack of significant changes to the G, G′, and RBM modes of the Raman spectra suggest that solvent doping is not responsible for the changes to fluorescence emission intensity observed in Figures 4-5 (B) and 4-5 (D). [99-101]

One plausible explanation is that the fluorescence of the large diameter SWNTs in SDS-suspended SWNTs was quenched in the initial suspension. It is generally accepted that exposure of the nanotube to protons in the aqueous phase quenches the exciton. [85, 88-91] The surfactant shell surrounding the nanotube, therefore, provides the needed protection to prevent non-radiative recombination of the exciton. Okazaki et al. [78] observed different ratios of the fluorescence emission intensities of SWNTs suspended in SDS to SWNTs in air leading them to conclude that SDS did not suspend larger diameter nanotubes. This conclusion is supported by the fact that smaller diameter SWNTs have stronger binding energies to SDS. [102] Researchers have observed that larger diameter SWNTs coated with SDS have a higher sensitivity to quenching. [91] Indeed, the initial SDS-suspensions have lower fluorescence intensities for larger diameter SWNTs in comparison to the initial SDBS-suspensions, as seen in Figures 4-4 (C) and 4-4 (D). Therefore, these intensity differences could mean that the largest diameter nanotubes have either (1) inadequate surfactant shells to aid dispersion and are truly not present

or (2) incomplete or non-uniform surfactant structures surrounding the nanotubes, which quench the emission fluorescence.

4.3.2 Possible Quenching Mechanism

Wallace and Sansom [20] showed through MD simulations that surfactant coverage was non-uniform and the thickness varied along the length of the nanotube. In other words, the surfactant permeability to protons from the water could potentially be altered as the surfactant concentration is changed, affecting fluorescence intensity. Others have also speculated similar 'holes' in the surfactant layer to help explain fluorescence behavior. [89, 91] If the permeability of the surfactant structure were altered, then these potential quenching spots could be removed, resulting in increased emission intensity. These alterations could occur by introducing solvents to protect the nanotube or by reorganization or redistribution of the surfactant surrounding SWNTs. These changes to the SDS surfactant structure should be most sensitive to the largest diameter SWNTs.

To test if solvents can improve the ability of the surfactant to protect the SWNT from quenching protons, the pH of the aqueous phase was adjusted to control the concentration of protons (fluorescence quenchers) while the organic solvent was still present and after the solvent is evaporated. As shown in Figures 4-7 (B) and 4-7 (C), the fluorescence intensity from the (7, 6) and (10, 5) SWNT types in a pure SDS-SWNT suspension decrease by two orders of magnitude at acidic pH similar to previous observations. [89, 91] However, the aqueous SWNT suspensions with the organic solvents forming a shell around the nanotubes have different trends from the pure SDS-SWNTs. The aqueous suspension mixed with benzene shows that the SWNTs are more resistant to pH changes. This resistance suggests that benzene offers another protective layer around the nanotube, providing further support for a swelled micelle state surrounding the SWNTs. On the other hand, suspensions mixed with ODCB showed more susceptibility to pH

quenching effects across the entire pH range. Only at pH values above 10, does the fluorescence intensity start to recover. These results suggest that the surfactant structure has become more permeable to quenching by protons or water, [89, 91] indicating that the nanotube surfactant structure has been altered or reorganized. Once again, the trends of all SWNT suspensions after solvent evaporation are similar to that of pure SDS as shown in Figures 4-7 (D) and 4-7 (E), which indicates that the surfactant structure has been recovered to a state similar to the initial state. However, there are some noticeable differences in the pH response. For the (7, 6) nanotube, ODCB provides some improvement to quenching in pH values near neutrality while benzene also shows improvements with slightly better fluorescence intensity at acidic pH values. In contrast, the larger diameter (10, 5) nanotube in Figure 4-7 (E) shows significant improvement in fluorescence emission intensity. SDS-SWNT suspensions exposed to benzene show significant improvement at pH values between 5 and 10. ODCB exposed nanotube suspensions show even better protection to the quenching effects of acid. This organic solvent improves the fluorescence intensity across the entire pH range but most notably for the acidic pH values.

The physisorption of surfactant molecules on nanotubes is a dynamic process, continuously being interchanged with free surfactant in solution. The introduction of an organic phase may alter this process. Indeed, surfactant molecules have slower desorption kinetics in emulsions than in micelles. [103] The organic phase may also enable increased mobility of the surfactant around the nanotubes. Depending on the interactions and their strengths, the surfactant reorganization may result in beneficial or detrimental effects to the fluorescence emission. These differences in surfactant-solvent-SWNT interactions helps explain the difference in spectra seen for SDS-suspensions in Figure 4-4. While benzene appears to swell the micelle, the other solvents open holes, enabling quenching from the aqueous phase. Upon evaporation of the

solvent, the surfactant structure can also be altered, which can improve the resistance to quenching and the fluorescence emission intensity. Table 4-2 summarizes these increases in intensity, which is also directly related to increases in their quantum yield since absorbance changes are relatively minor. The intensity increases are most significant for the largest diameter nanotubes. Chloroform tends to improve the fluorescence emission intensity more than ODCB. The largest emission increases are observed for the (11, 3), (10, 5), and (9, 7) SWNT types, which have a 107.1%, 179.3%, and 177.6% increase in intensity, respectively.

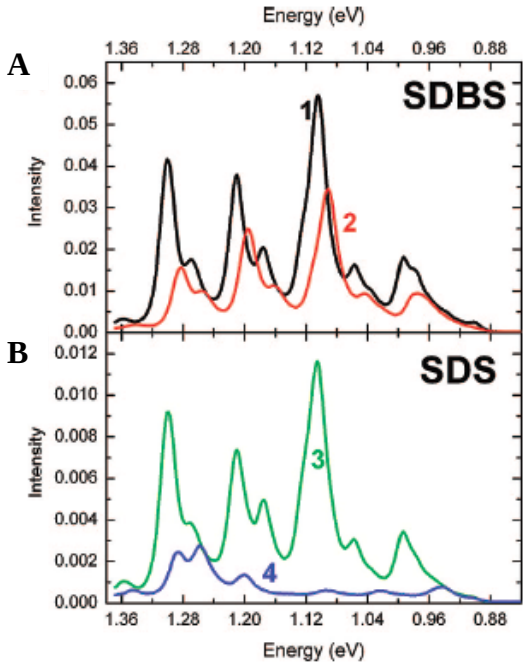

Figure 4-1. Comparison of NIR fluorescence spectra (ex = 662 nm) of surfactant-coated SWNT suspensions before (**1** and **3**) and after mixing with ODCB (**2** and **4**). A) SDBS-suspended SWNTs and B) SDS-suspended SWNTs.

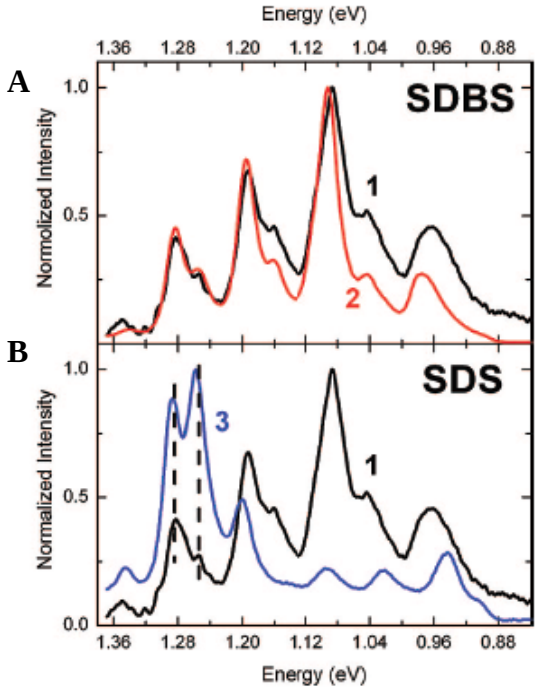

Figure 4-2. Comparison of normalized NIR fluorescence spectra (ex = 662 nm) of surfactant-coated SWNT suspensions to SWNTs dispersed in only ODCB (**1**). A) SDBS-SWNTs (**2**) and B) SDS-SWNTs (**3**) after mixing with ODCB.

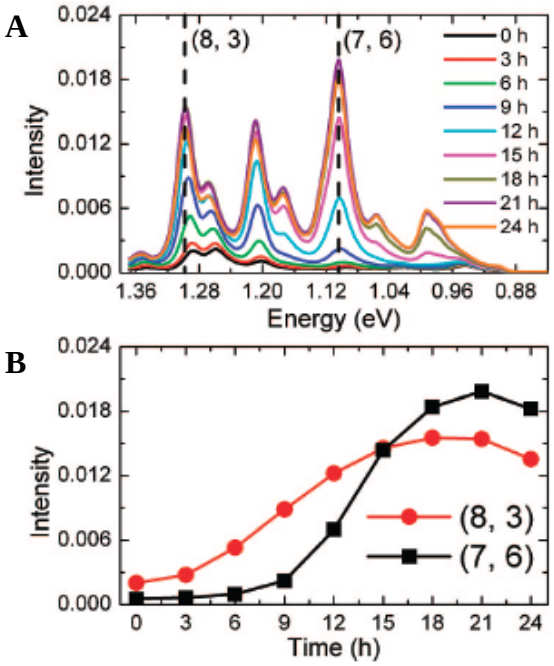

Figure 4-3. A) NIR fluorescence spectra (ex = 662 nm) of SDS-coated SWNT suspensions mixed with ODCB during solvent evaporation. B) Time-dependent recovery of (7, 6) and (8, 3) peak intensities of SDS-SWNTs mixed with ODCB.

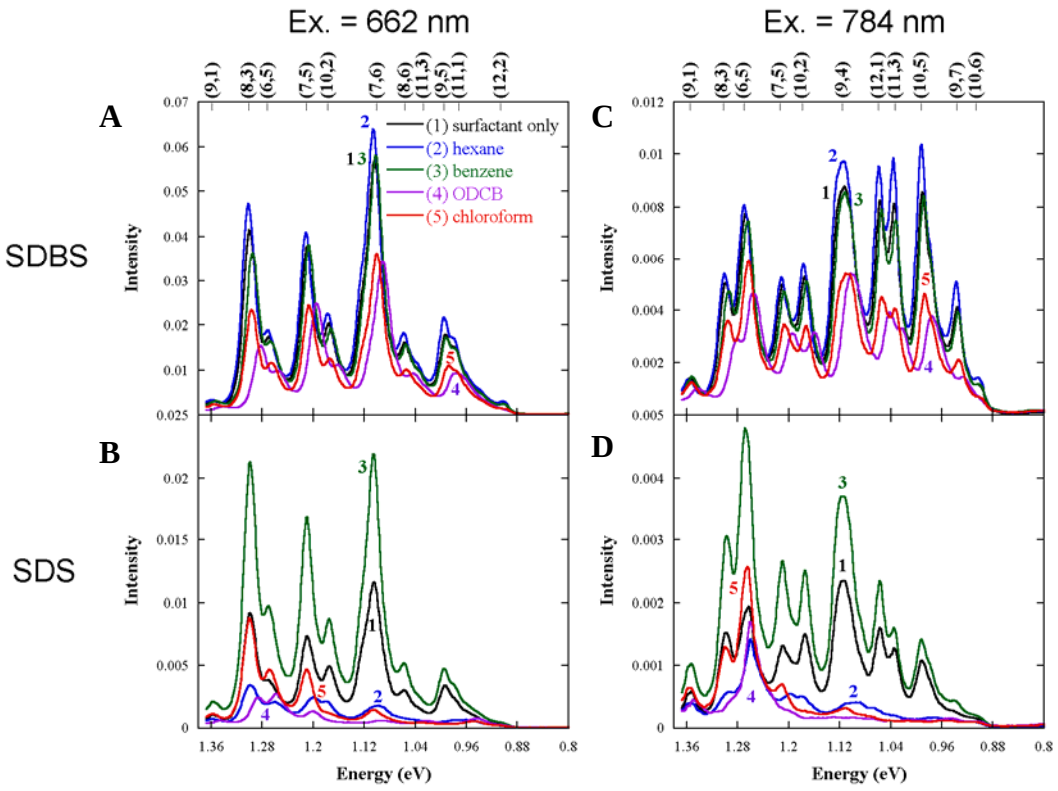

Figure 4-4. NIR fluorescence spectra of SDBS- and SDS-coated SWNT suspensions after being mixed with the immiscible organic solvents: hexane (**2**), benzene (**3**), ODCB (**4**), or chloroform (**5**). The initial surfactant-SWNT suspension (**1**) is plotted for comparison. Excitation from 662 and 784 nm lasers.

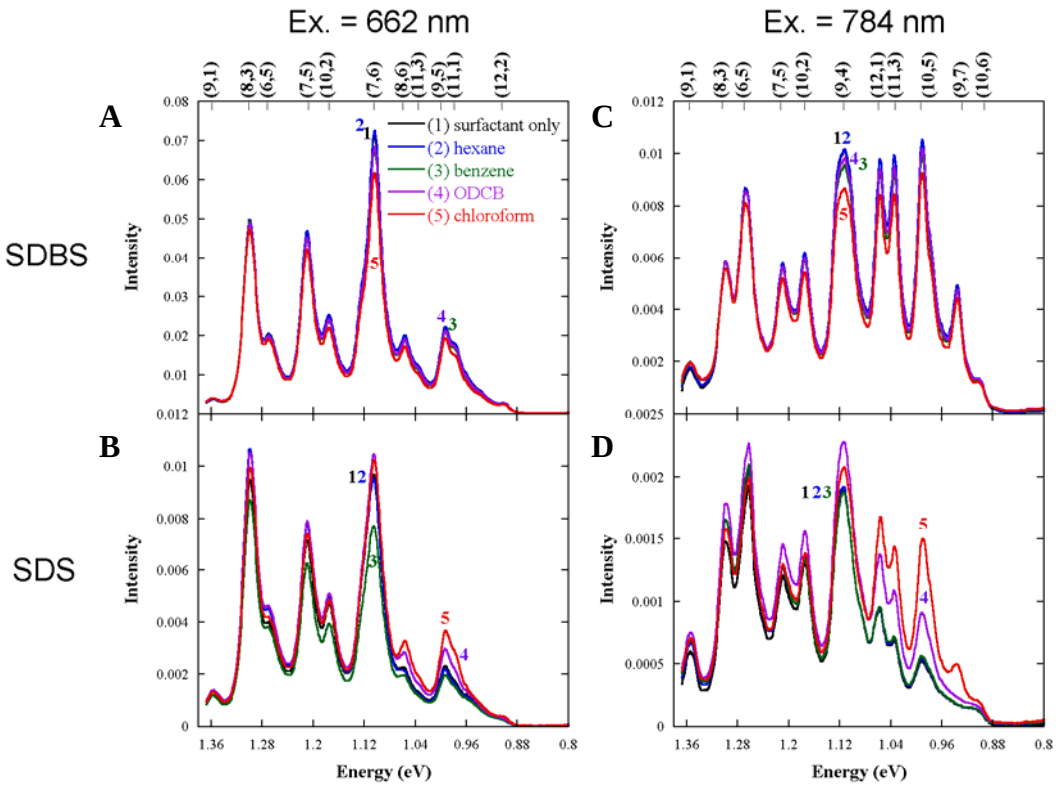

Figure 4-5. NIR fluorescence spectra of SDBS- and SDS-coated SWNT suspensions after evaporation of the immiscible organic solvents: hexane (**2**), benzene (**3**), ODCB (**4**), or chloroform (**5**). The surfactant-SWNT suspension exposed to air for 24 h (**1**) is plotted for comparison. Note that both SDS- and SDBS-coated SWNT suspensions showed minor changes to the emission spectra after being open to air for 24 h. Excitation from 662 and 784 nm lasers.

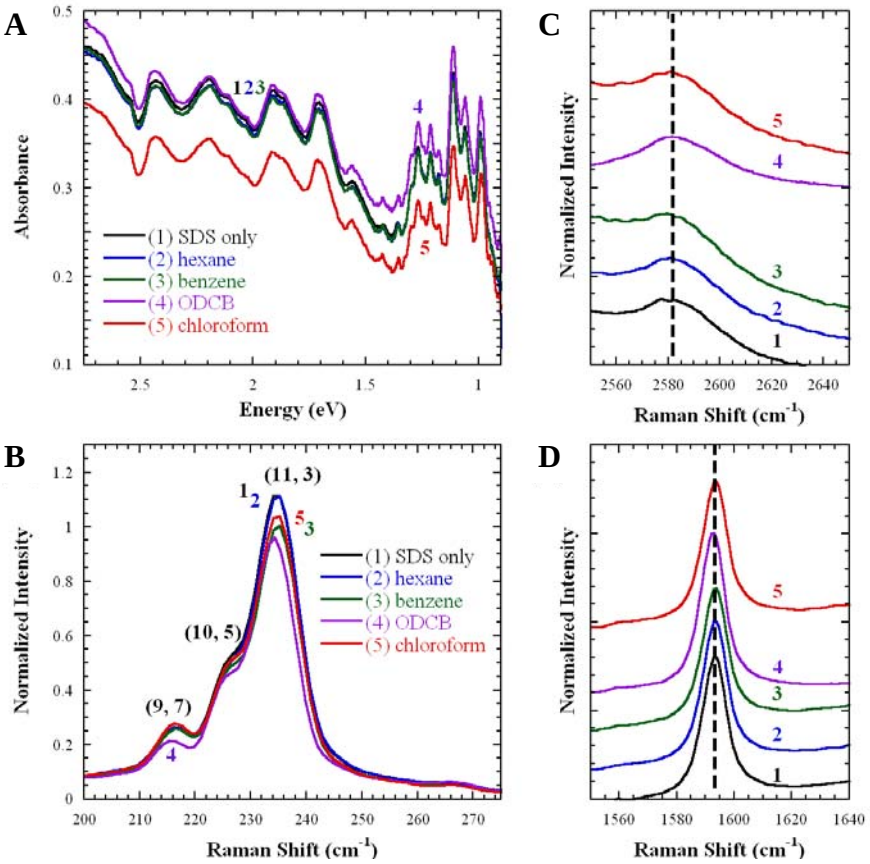

Figure 4-6. A) Absorbance and (b–d) Raman spectra (ex = 785 nm) of SDS-coated SWNT suspensions after evaporation of the organic solvent: hexane (**2**), benzene (**3**), ODCB (**4**), or chloroform (**5**). The surfactant-SWNT suspension exposed to air for 24 h (**1**) is plotted for comparison. The radial breathing modes (RBMs) for specific (*n*, *m*) SWNT types are shown in B) while C) and D) show the Raman spectrum of the G′ and G band of the SDS-coated SWNTs suspensions, respectively. The dashed lines indicate the positions of the surfactant suspensions prior to mixing with organic solvents. All spectra in C) and D) are offset for clarity.

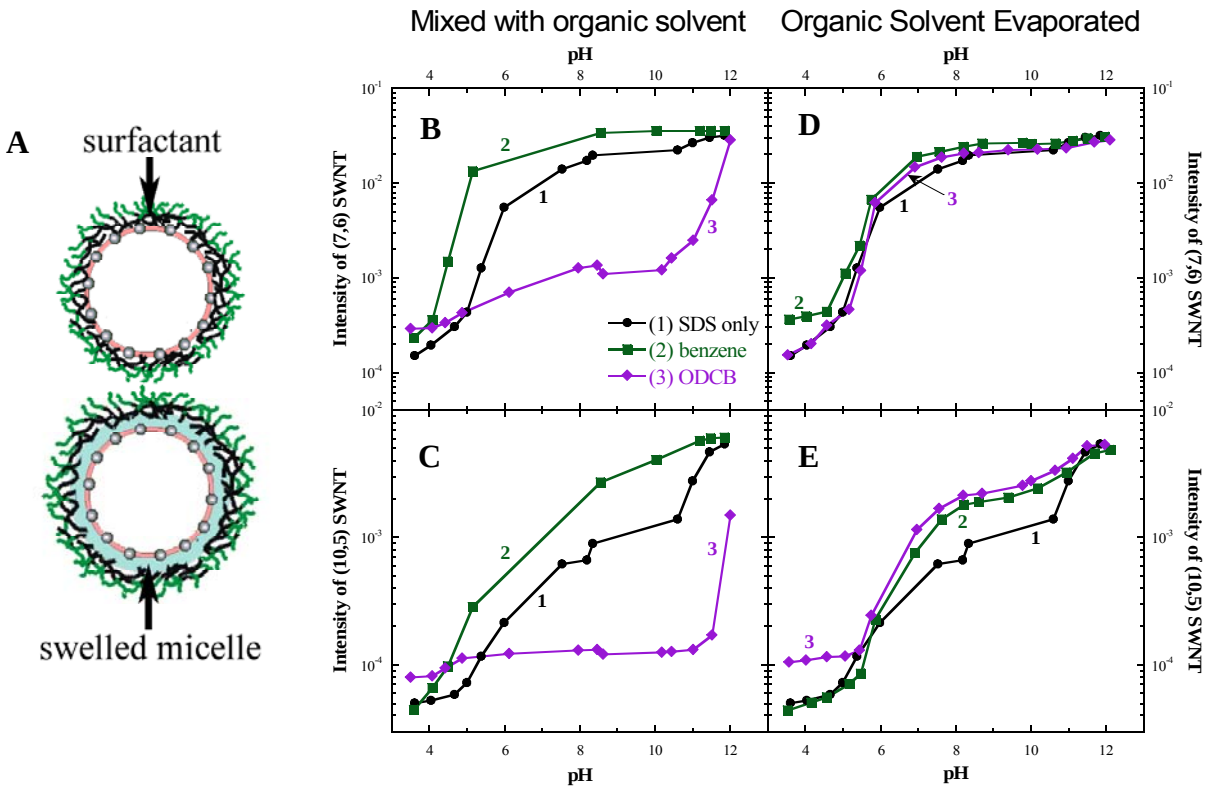

Figure 4-7. A) Swelling of the hydrophobic core of the micelle surrounding SWNTs. B)-E) The effect of pH on the fluorescence intensity of the (7, 6) SWNT (ex = 662 nm) and (10, 5) SWNT (ex = 784 nm) in SDS-suspensions after being mixed with the immiscible organic solvents benzene and ODCB and after evaporation of the solvent.

Table 4-1. Spectral changes of surfactant-coated SWNTs mixed with organic solvents.

Organic Solvent	Dielectric Constant[a]	Dipole Moment (D)[a]	**SDBS-SWNTs**		**SDS-SWNTs**	
			Fluorescence Intensity Change	Solvatochromic Shift Change	Fluorescence Intensity Change	Solvatochromic Shift Change
Hexane	1.89	0	small increase	blue	large decrease	red
Benzene	2.28	0	varied	red	large increase	slight blue
Chloroform	4.81	1.04	decrease	red	varied	varied
ODCB	10.12	2.50	decrease	red	large decrease	red
water	80.1	1.85	—	—	—	—

[a] *Values taken from the CRC Handbook of Chemistry and Physics*

Table 4-2. Fluorescence intensity changes for various SWNT (*n*, *m*) types after exposure to ODCB or chloroform.

SWNT	Diameter (nm)	Intensity Increase (%) ODCB	chloroform
(7,6)[a]	0.895	8.3	6.0
(9,4)[b]	0.916	20.6	10.1
(8,6)[a]	0.966	24.9	42.4
(9,5)[a]	0.976	27.9	57.5
(12,1)[b]	0.995	46.0	75.9
(11,3)[b]	1.014	56.8	107.1
(10,5)[b]	1.050	72.4	179.3
(9,7)[b]	1.103	34.6	177.6

[a] *Excitation from 662 nm laser*

[b] *Excitation from 784 nm laser*

CHAPTER 5
SOLVATOCHROMIC EFFECTS OF SWNTS IN NONPOLAR MICROENVIRONMENTS

Single-walled carbon nanotubes (SWNTs) have unique properties suitable for a wide variety of applications. [4, 5] However, characterizing the properties of SWNTs has been difficult because of the ensemble of nanotubes present in a suspension. [104] Further complicating the characterization of SWNT properties is the inability to suspend SWNTs in known dielectric environments, such as organic solvents. [36] Dispersing SWNTs with the aid of surfactants has significantly advanced SWNT characterization. For example, the unique photoluminescence (PL) emission of semiconducting SWNTs can identify the (n, m) types in a suspension. [2] However, an incomplete understanding of the surface coverage and structure of surfactants surrounding SWNTs makes it difficult to assess the dielectric constant of the media surrounding SWNTs. [105] The unknown environment surrounding SWNTs poses problems to characterizing and separating SWNTs through dielectrophoresis, and using SWNTs in sensing applications. [27, 76, 89, 91]

The polarizability of individual SWNTs is important to many applications as well as the photophysical and photochemical response of SWNTs. The polarizability is highly anisotropic with the longitudinal component ($\alpha_{\parallel}$) at least an order of magnitude larger than the transverse component ($\alpha_{\perp}$). Therefore, the longitudinal polarizability is the dominant contribution and the dipole moment is oriented along the nanotube axis. Several models have been developed to calculate the longitudinal polarizability. These simulations suggest the longitudinal polarizability is a function of the nanotube radius and band gap energy of SWNTs but disagree on the relationship. Researchers have found that the longitudinal polarizability is proportional to radius over band gap squared, [106] inverse band gap, [107] inverse band gap squared, [108] and radius squared. [109]

While there are several theoretical studies on polarizability, there are few experimental studies. [110, 111] Measuring the photophysical properties of molecules, such as solvatochromic shifts, can provide information about the excited states of the molecules and even their polarizability. Choi and Strano used solvatochromic shifts of SWNTs to determine that longitudinal polarizability varies with inverse nanotube radius times inverse band gap squared. [110] However, these measurements were based on relatively few systems including surfactant-suspended SWNTs, which have unknown dielectric environments around nanotubes.

The theoretical and experimental studies described above show that the exact form of the longitudinal polarizability remains unknown. Experimental measurement of solvatochromic shifts in a variety of solvents remains a good approach to study polarizability, provided that SWNTs can be suspended in several solvents of known dielectric constant. Our group has observed that mixing a suspension containing sodium dodecylbenzenesulfonate (SDBS)-coated SWNTs with immiscible organic solvents induces solvatochromic shifts dependent on the solvent. [76] The fluorescence spectra of SDBS-SWNT suspensions mixed with o-dichlorobenzene (ODCB) showed identical shifts to the PL from SWNTs suspended in only ODCB (i.e., no surfactant or water). [36] The similarity in the peak positions indicates that the hydrophobic core of the surfactant forms an emulsion-like environment of ODCB around the nanotube.

In this chapter, we describe using these new microenvironments around SWNTs to investigate the photophysical properties of SWNTs in a variety of solvents and mixtures. The solvatochromic shifts follow the expected behavior from a polarizable solute in a polarizable solvent. The fluorescence intensity is shown to be very sensitive to small concentrations of polar

components. The peak positions of known solvent environments are then used to describe the dielectric media in surfactant-coated SWNT suspensions.

5.1 Experimental Procedure

5.1.1 Dispersion

All experiments used SDBS since this surfactant did not demonstrate any changes to the surfactant structure upon mixing with organic solvents, as observed for SDS-SWNT suspensions [76]. SWNT suspensions (Rice HPR 145.1) were prepared in 1 wt% SDBS solutions followed by ultracentrifugation. Aqueous suspensions of nanotubes were prepared by mixing 20 mg of raw SWNTs with 200 mL of a sodium dodecylbenzene sulfonate (SDBS) solution (1 wt.%). High-shear homogenization (IKA T-25 Ultra-Turrax) for 1.5 – 2 h and ultrasonication (Misonix S3000) for 10 min were used to aid dispersion. After ultrasonication, the mixture was ultracentrifuged at 20,000 rpm for 5 h (Beckman Coulter Optima L-80 K). Immiscible solvents were added to each SWNT suspension (solvent: water volume ratio of 0.5) and mixed. The dielectric constant, refractive index, dipole moment, and induction polarization for each solvent is given in Table 5-1. The mixture was shaken vigorously for 30 s with a vortex stirrer. A white emulsion phase immediately started to phase separate after shaking. After waiting for 1.5 – 2 h to reach steady state, the excess organic solvent was then carefully removed from the aqueous SWNT suspension to prevent further emulsification. The mixtures of hexane and o-dichlorobenzene (ODCB) were prepared by mixing different molar ratios of each solvent prior to their interaction with aqueous SWNT suspensions. The same solvent: water volume ratio (0.5) and procedures were used to mix, separate and characterize the suspension.

5.1.2 Characterization

The aqueous phase was characterized by vis-NIR absorbance and NIR-fluorescence spectra using an Applied NanoFluorescence Nanospectrolyzer (Houston, TX) with excitation from 662

and 784 nm diode lasers. Although the organic solvents have some absorbance bands in the NIR region, their affect on the spectral properties were determined to be minor. This conclusion is supported by the fact that no changes to the absorbance spectra of SWNTs are observed, which is consistent with a very small volume of solvent in the system. Likewise, the presence of solvent was concluded to have minimal effects on the fluorescence emission intensity.

5.2 Results and Discussion

5.2.1 Solvatochromic Shifts

Figures 5-1 (A) and (B) show peak shifts of the PL spectra for the (7, 6) and (10, 5) SWNT types when mixed with a variety of nonpolar solvents having different dielectric constants, refractive index, and polarity. As seen in the figures, systematic changes are observed in both the intensity and peak position. These changes show that the emission energy red-shifts and the intensity decreases as the solvent polarity is increased from hexane to ODCB. In addition, the peak widths get broader in high polarity solvents, such as 3, 4–dichlorotoluene and ODCB. The absorbance spectra for both the E_{11} and E_{22} transitions of the (7, 6) SWNT shown in Figures 5-1 (C) and (D) also red-shift as the solvent polarity is increased. The E_{22} transitions are generally weaker than the E_{11} peak shifts, in agreement with prior observations. [110]

The peak shifts in the spectra of Figure 5-1 indicate that SWNTs are experiencing different environments when mixed with nonpolar organic solvents. SWNTs have no net dipole moment but are highly polarizable. The presence of different solvent environments around the SWNTs results in different reaction fields, which affect the absorbance spectra (Figures 5-1 (C) and (D)). The excited state of SWNTs after photon absorption forces the solvent structure to rearrange around the excited state SWNT dipole. The change in solvent orientation establishes slightly different reaction fields around the SWNTs, resulting in solvatochromic shifts of the fluorescence emission of SWNTs (Figures 5-1 (A) and (B)) that differ from those observed in

absorbance. The observed spectral changes in Figure 5-1 suggest the measured solvatochromic shifts are due to the formation of a solvent microenvironment encapsulating the SWNTs.

Different ratios of hexane and ODCB were prepared and mixed with the aqueous SWNT suspension to verify that a microenvironment encapsulating the SWNTs forms. The polarity and dielectric constant of hexane and ODCB are the lowest and highest, respectively, of all solvents used in Figure 5-1. The fluorescence spectra for each mixture is shown in Figure 5-2 (A) for the (10, 5) SWNT. Pure hexane shows the highest fluorescence intensity and largest emission energy. As the fraction of ODCB in the mixture increases, the fluorescence intensity steadily decreases while the peak position red-shifts. These trends continue until the spectra converge to that observed for pure ODCB. In "ideal" non-associating solvent mixtures, the solvatochromic shift should follow a simple mixing rule, yielding a linear trend of the solvatochromic shift as a function of mole fraction. [112] Figure 5-2 (B) shows that the peak shift for multiple (n, m) types are indeed linear, demonstrating that systematic changes to the solvent environment around SWNTs is occurring.

The PL intensity of each SWNT type, however, shows non-linear behavior. The fluorescence intensity quickly falls as the fraction of ODCB is increased. These intensity decreases are dependent on the SWNT diameter. For example, the fluorescence emission intensity of small diameter SWNTs (e.g. (8, 3) types) decrease by approximately 60% while the fluorescence of large diameters (e.g. (10, 5) types) decrease by 80%. These results also show that SWNT fluorescence emission is very sensitive to even small amounts of a more polar solvent (the intensity decreases by approximately 50% at $x_{ODCB} \approx 0.2$). This sensitivity could have significant implications in understanding the fluorescence emission intensity from aqueous suspensions, where minor amounts of water in contact with the SWNT sidewall may

significantly affect fluorescence intensity. Indeed, researchers have found that better surfactant layers result in higher fluorescence intensity. [76, 89]

5.2.2 SWNT-Solvent Interaction

The solvents used for these experiments are all considered to be nonpolar because of the relatively low dielectric constants. [113] Therefore, the solvatochromic shifts for each solvent are primarily influenced by the polarizability–polarizability interactions given by [98, 112]:

$$\Delta E_{11} = E_{11}^{air} - E_{11}^{solvent} = -C_{solvent} \frac{\Delta\alpha_{11}}{\beta\gamma a^3} \Delta f_{air-solvent} \tag{5-1}$$

where $C_{solvent}$ is a fluctuation parameter associated with SWNT dispersion forces, $\Delta\alpha_{11}$ is the change in polarizability of SWNTs between the ground and excited states, β is a shape factor for the SWNT, γ is a parameter associated with the location of the SWNT dipole in the volume a^3, and Δf is the solvent induction polarization described by the Onsager polarity functions, $f(\eta^2) = 2(\eta^2 - 1)/(2\eta^2 + 1)$. [98, 112] Figure 5-3 shows the measured PL peak shifts from the data in Figure 5-1 relative to air for multiple (n, m) types as a function of $f(\eta^2)$. The solvatochromic shifts (ΔE_{11}) are larger for the small diameter (large band gap) SWNTs. The solvatochromic shifts also tend to be linear as expected from equation (5-1). However, the solvatochromic shifts start to exhibit non-linear behavior at high $f(\eta^2)$. The general solvent effect models used here ignore higher order terms, such as dipole moments induced in the solvent molecules by the SWNTs and vice versa. [98, 112] These effects are expected to yield a curved relationship to the solvatochromic shift plots shown in Figure 5-3. [112] The largest deviations are for those solvents that possess a small dipole.

The E_{ii} transitions for each (n, m) SWNT type from either the fluorescence or absorbance spectra can be used to estimate the SWNT polarizability or its functional form; however, the fluorescence data is used because the (n, m) peaks are better resolved. Previously, Choi and Strano [110] concluded that the difference in SWNT polarizability used in equation (5-1) is primarily determined by the longitudinal polarizability of the exciton (i.e., $\Delta\alpha_{11} \approx \alpha_{11,||}$). Several research groups have described the longitudinal polarizability of each SWNT (n, m) type by a function of the form, $\alpha_{11,||} = kR^a E_{11}^b$, where k is a constant, R is the SWNT radius, E_{11} is the band gap as measured in air, and a and b are integers. [106-109] As described above, there is no consensus on the relationship (i.e., constants a and b) for the polarizability. If the volume associated with the solvent reaction field is assumed to have a radius equivalent to the SWNT radius, then equation (5-1) becomes:

$$\Delta E_{11} = \frac{-C_{solvent}}{\beta\gamma} kR^{a-3} E_{11}^b \Delta f = -D_{solvent} R^{a-3} E_{11}^b \Delta f \qquad (5\text{-}2)$$

For simplicity, the constants $C_{solvent}$, k, β, and γ are combined into one constant $D_{solvent}$. Since equation (5-2) is valid for all solvents, the measured solvatochromic shifts in Figure 5-3 can then be compared to this equation to determine the global variables, a and b, and the solvent specific variables, $D_{solvent}$.

All fluorescence spectra in Figure 5-1 were deconvoluted into their respective (n, m) peaks. Details of the deconvolution and fitting procedure are given in the supporting information. Briefly, the confidence level of each peak in the deconvoluted spectra was evaluated to assess its relative importance in regression analysis. This approach is chosen because of the disparity in peak intensity and overlap. For example, the fluorescence peak associated with the (7, 6) SWNT type typically has high intensity and little overlap with other (n, m) SWNT types while the (12,

2) SWNT peak often has low intensity and significant overlap. Therefore, more confidence should be assigned to peak parameters and solvatochromic effects for the (7, 6) SWNT type because of its intensity and separation from other peaks. However, the fluorescence spectra of other SWNT types still contains important information. To account for the varying confidence levels in each deconvoluted peak, weighting factors were assigned based on the relative intensity and amount of overlap. A constrained nonlinear optimization model was then formulated using the generalized reduced gradient (GRG) method. [114] An objective function (ϕ) was chosen to be the squared sum of residuals multiplied by the weighting factors (w_i) where ΔE_{11} are the measured shifts relative to air or the calculated values from equation (5-1). These residuals were summed over all (n, m) types and solvents to obtain the final objective function:

$$\min \phi = \sum^{\text{all solvents}} \sum^{\text{all } n,m} w^{n,m}_{Intensity} w^{n,m}_{Overlap} \left(\Delta E^{n,m}_{11,measured} - \Delta E^{n,m}_{11,calculated} \right)^2 \qquad (5\text{-}3)$$

The objective function (5-3) was first solved for each solvent independently. The fluorescence emission data from all solvent systems was then included in the objective function to obtain the parameters a, b, and $D_{solvent}$. The regression analysis shows that the global solution and 11 of 16 single-solvent optimization solutions yield $a = -2$ and $b = -3$. These results deviate from prior experimental and computation results, which obtained values of a ranging from 2 to –1 and b from 0 to –2. [106-109] However, note that those solutions that deviate from the other results tend to be the most polar solvents. The changes in intensity and peak position for these systems induce more error in peak assignment. On the other hand, some of these systems give a and b constants comparable to those obtained before. [107, 110]

The known solvatochromic shifts of SWNTs in solvents can be used to probe unknown environments. [98] This approach may be particularly useful in understanding the structure of

surfactants surrounding SWNTs, which still remains unknown. [20, 76, 105] Figure 5-4 shows the peak position of fluorescence emission from (7, 6) SWNTs surrounded by the surfactants SC, SDBS, SDS, and CTAB relative to the positions in different solvent microenvironments. The peak positions for SC- and SDBS-coated SWNTs are similar to those measured in alkanes and other low dielectric media. These results suggest that SC and SDBS molecules are oriented such that the hydrocarbon backbone is in contact with the nanotube sidewall and the anionic groups are extended away from the SWNT. On the other hand, the peak positions of SDS and CTAB show considerable red-shifts and have environments that are similar to the relatively high dielectric media of 3, 4-dichlorotoluene and ODCB. These two surfactants have long chain alkanes as the backbone (hexadecane and dodecane) and these systems would be expected to have similar peak positions as the alkane solvents and SDBS. These deviations suggest the surfactant structures for SDS- and CTAB-coated SWNTs differ from the SC- and SDBS-based systems. The red-shifts of the fluorescence spectra could indicate that the anionic groups are in close proximity to the nanotube sidewall [105] or that the surfactant structure does not adequately cover the nanotube, [76, 105] allowing significant interactions with water.

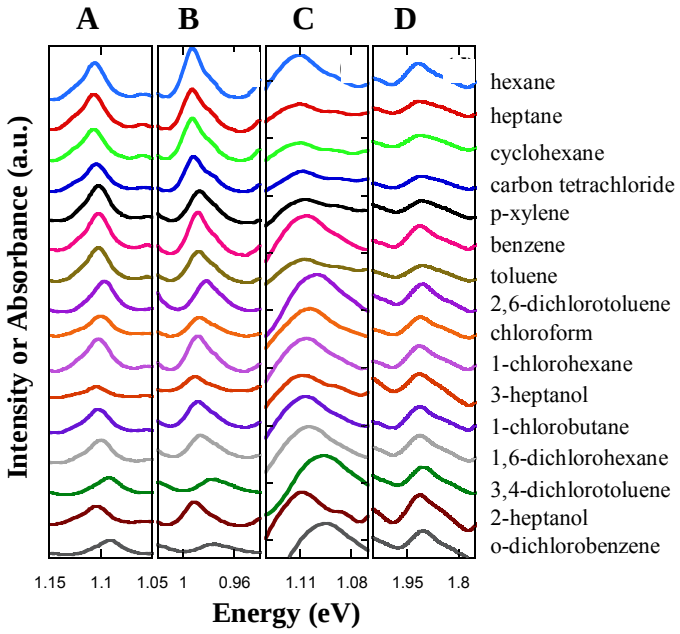

Figure 5-1. PL spectra (E_{11} emission) for the A) (7, 6) and B) (10, 5) SWNT types and C) E_{11} and D) E_{22} absorbance for the (7, 6) SWNT type measured in microenvironments of various nonpolar solvents.

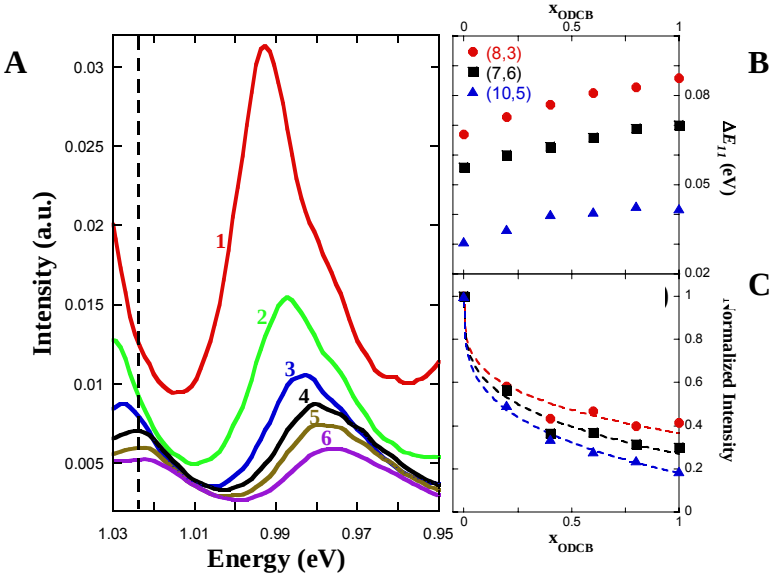

Figure 5-2. A) The PL emission spectra for the (10, 5) SWNT in a hexane/ODCB mixture at different mole fractions of ODCB: (**1**) $x_{ODCB} = 0.0$; (**2**) $x_{ODCB} = 0.2$; (**3**) $x_{ODCB} = 0.4$; (**4**) $x_{ODCB} = 0.6$; (**5**) $x_{ODCB} = 0.8$; (**6**) $x_{ODCB} = 1.0$. The dashed line is the position of the E_{11} emission energy in air. The B) peak shift (relative to air not the initial SDBS suspension) and C) intensity changes for multiple (n, m) types at different mole fractions of ODCB in a hexane/ODCB mixture. The dashed line in C) are guides to show the trend.

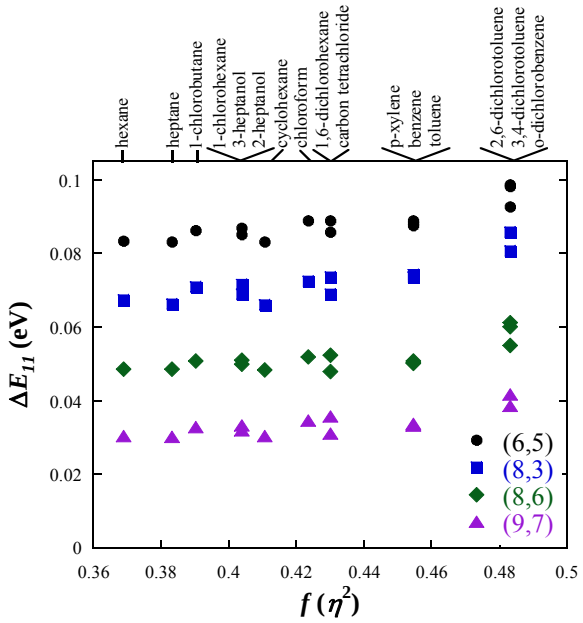

Figure 5-3. Solvatochromic shifts of various (n, m) SWNT types in nonpolar solvents with different solvent induction polarization, $f(\eta^2)$.

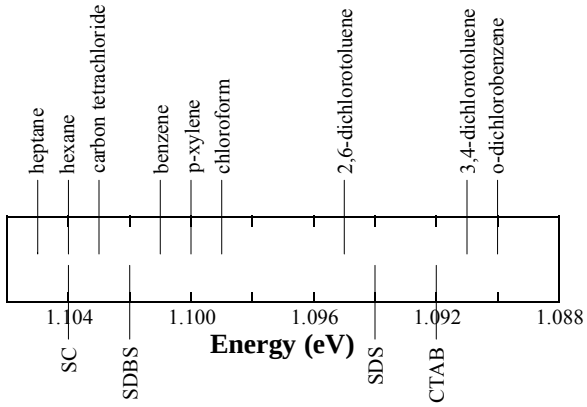

Figure 5-4. Comparison of the peak positions for the (7, 6) SWNT type suspended in surfactants and suspended in sodium dodecylbenzenesulfonate (SDBS) but surrounded by various nonpolar solvents. Sodium cholate (SC), sodium dodecylbenzenesulfonate (SDBS), sodium dodecyl sulfate (SDS), and cetyl trimethylammonium bromide (CTAB).

Table 5-1 Solvent Parameters

Solvents	Dielectric Constant[a]	Refractive Index[a]	Dipole Moment	Induction Polarization $f(\eta^2)$
hexane	1.89	1.37	0.00[a]	0.369
heptane	1.92	1.39	0.00[a]	0.383
cyclohexane	2.02	1.43	0.00[a]	0.411
carbon tetrachloride	2.23	1.46	0.00[a]	0.430
p-xylene	2.27	1.50	0.00[a]	0.455
benzene	2.28	1.50	0.00[a]	0.455
toluene	2.39	1.50	0.38[a]	0.455
2, 6-dichlorotoluene	3.36	1.55	0.83[b]	0.483
chloroform	4.81	1.45	1.04[a]	0.424
1-chlorohexane	6.10	1.42	1.94[a]	0.404
3-heptanol	7.07	1.42	1.71[a]	0.404
1-chlorobutane	7.28	1.40	2.05[a]	0.390
1, 6-dichlorohexane	8.60	1.46	2.03[c]	0.430
3, 4-dichlorotoluene	9.39	1.55	3.00[a]	0.483
2-heptanol	9.72	1.42	1.71[a]	0.404
o-dichlorobenzene	10.12	1.55	2.50[a]	0.483

[a] Values taken from CRC Handbook of Chemistry and Physics [115]
[b] Values taken from Calderbank et al. [116]
[c] Values taken from Vaughan et al. [117]

CHAPTER 6
CONCLUSIONS AND RECOMMENDATIONS

This dissertation covers three research topics that are important to the application of SWNTs. The conclusions associated with the removal of SWNT bundles are presented in Section 6.1. The conclusions associated with the nonpolar microenvironment around SWNTs are presented in Section 6.2. The conclusions associated with the solvatochromism of SWNTs are presented in Section 6.3. The recommendations for further study are presented in Section 6.4.

6.1 Removing SWNT Bundles via Interfacial Trapping

SWNT bundles can be removed from an aqueous suspension of individual SWNTs by interfacial trapping. This technique offers a simple route to achieve large-scale production of aqueous SWNT suspensions. The significant decrease in absorbance intensity and the Raman aggregation peak combined with increases in fluorescence intensity suggests that nanotube bundles are selectively removed from the aqueous suspension. Although the quality of SWNT dispersions of a single interfacial trapping step is lower than that of the established ultracentrifugation method, different processing conditions and multiple extraction steps improve the dispersion quality, making it comparable to ultracentrifugation. A simple model is developed to describe the changes in free energy and helps explain why SWNT bundles preferentially exist at the interface, yielding effective separations.

The removal of SWNT bundles through the IT process is based on selective partitioning at liquid-liquid interfaces. However, the ionic groups on typical surfactants used to disperse SWNTs poses problems for trapping SWNT bundles at the interface. Efficient trapping of SWNT bundles at interfaces is achieved by adjusting the surface charge. Zeta potential measurements show that a minimum surface charge occurs at pH 6.75, which correlates to the most efficient IT separations. A pH-adjusted two-step IT process is shown to yield SWNT

suspensions comparable in dispersion quality to suspensions prepared by ultracentrifugation. Most importantly, the IT process is a simple and fast approach with double the yield of suspended SWNT material when compared to the conventional ultracentrifugation method. Further, the IT process can be easily scaled-up to provide substantial throughput.

6.2 Nonpolar Microenvironments Around SWNTs

The hydrophobic core of the surfactant structure surrounding SWNTs can be swelled with immiscible organic solvents. These swelled states could be either a continuous or discontinuous organic layer that results in significant changes to the fluorescence and absorbance spectra. The spectral shifts are reversible, disappearing once the solvent is removed. However, some surfactant-solvent systems show permanent increases to fluorescence emission intensity, which cannot be attributed to changes in concentration, dispersion, or doping. These permanent changes to emission intensity are attributed to surfactant reorganization, which helps eliminate fluorescence quenching from the aqueous phase. These results may have important implications in processing SWNT suspensions and analyzing the fluorescence of SWNT suspensions. For example, the exposure of SWNTs to small amounts of organic solvents may give the illusion that separation has occurred as seen in Figures 4-1 (B), 4-4 (B), and 4-4 (D). Finally, the changes in fluorescence attributed to surfactant reorganization suggest that changes to processing conditions may yield improved fluorescence intensity (quantum yields) of bulk SWNT suspensions.

6.3 Solvatochromism of SWNTs

We also demonstrate that multiple solvents form microenvironments around SWNTs with characteristic solvatochromic shifts. The shifts scale well with the solvent induction polarization, $f(\eta^2)$, as expected for interactions of a polarizable SWNT with a polarizable solvent. In addition, solvent mixtures follow the expected trends and also show the sensitivity of SWNT fluorescence to slightly polar solvents. A constrained nonlinear optimization model was used to study the

polarizability changes with each solvent microenvironment. The results yield a longitudinal polarizability of the form $\alpha_{11,\|} \propto 1/(R^2 E_{11}{}^3)$.

6.4 Recommendations

Future work should focus on expanding the combination of surfactants and solvents that can produce high-quality dispersions of individual SWNTs by interfacial trapping. This database of viable surfactants and solvents will be beneficial to both industry and academia since the interfacial trapping method is scalable and economical. These studies may also lead to a better understanding of the factors that determine the formation of solvent microenvironments around SWNTs and how the surfactant reorganizes upon solvent evaporation.

Another possible future work should be the sensing devices based on the unique NIR-fluorescence properties of SWNTs. Our work has shown that the fluorescence can be improved after the treatment of immiscible organic solvents. Therefore, this improvement can be utilized in biosensing and bioimaging fields since the fluorescence are widely applied in these research areas. The surfactant structure can be reorganized to protect SWNTs from extrinsic quenching mechanism after liquid-liquid interactions to increase the quantum yields of SWNTs. The increased quantum yields of nanotubes should help the efficiency and accuracy of the imaging and sensing in medical treatment.

APPENDIX A
SUPPORTING INFORMATION FOR INTERFACIAL TRAPPING OF SWNT BUNDLES

A.1 Optical Linearity

In order to interpret concentration changes in the spectra, the linear regions of the absorbance and fluorescence spectra were determined. A concentrated Gum Arabic SWNT suspension (1 mg/mL) was homogenized and ultrasonicated and then diluted with 1 wt% Gum Arabic solution. At each dilution step, the absorbance and fluorescence spectra were recorded. Figure A-1 (A) and Figure A-1 (B) show the absorbance at 763 nm and the intensity (by 662 nm excitation) of the most prominent peak corresponding to the (7, 6) SWNT type with the variation of the SWNT concentration, respectively.

The initial SWNT concentration strongly affected the absorbance and fluorescence values obtained. These effects could possibly be due to changes in equilibrium concentrations for individual and bundled SWNTs. [16] Regardless of the initial concentration, the fluorescence spectra showed a linear relation to concentrations of ~ 0.03 mg/mL. The linear response of the absorbance was dependent on the initial concentration. However, all absorbance spectra was linear to at least 0.1 mg/mL. All spectral data presented in the manuscript are within the linear regions.

A.2 Correction of Absorbance Spectra of SWNTs

In some cases, the absorbance spectra were corrected by subtracting the non-resonant background to obtain the spectra of individual SWNTs. The background was determined by the following equation:

$$A_{bg} = \frac{k}{\lambda^b} \tag{A-1}$$

where k and b are the empirical fit parameters. [118, 119]

Figure A-2 (A) represents the corrected spectra of SWNTs after single- and two-step interfacial trapping compared to ultracentrifugation. The spectra show that interfacial trapping does remove some individual SWNTs from the suspension but favors the removal of bundled SWNTs. By comparing the overall absorbance change between the single- and two-step interfacial trapping process (Figure 2-7 (B)) and the absorbance change of individual SWNTs (Figure A-2 (A)), it is estimated that only 15% of the total absorbance change in Figure 2-7 (B) is due to removal of individually suspended SWNTs. In addition, the final concentration of individual SWNTs in the two-step and ultracentrifuged suspensions are similar.

Figure A-2 (B) shows the corrected spectra of SWNTs after interfacial trapping using different oil-to-aqueous suspension volume ratios (R). The overall concentration of individual SWNTs is higher for water-in-oil (w/o) emulsion systems ($R > 1$) than oil-in-water emulsions ($R < 1$). However, the fraction of individual SWNTs in w/o systems is lower than o/w systems as shown in Figure 2-6 (B).

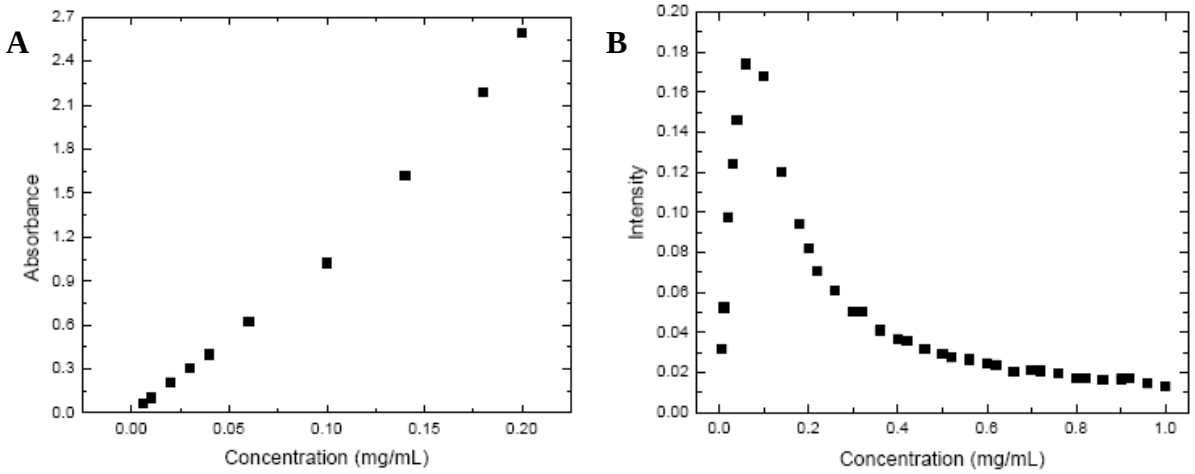

Figure A-1. A) Absorbance at 763 nm the (7, 6) SWNTs type as a function of nanotube concentration. Initial SWNT concentration of 1 mg/mL B) Fluorescence emission intensity the (7, 6) SWNT type (Ex. = 662 nm) as a function of nanotube concentration. Initial SWNT concentration of 1 mg/mL

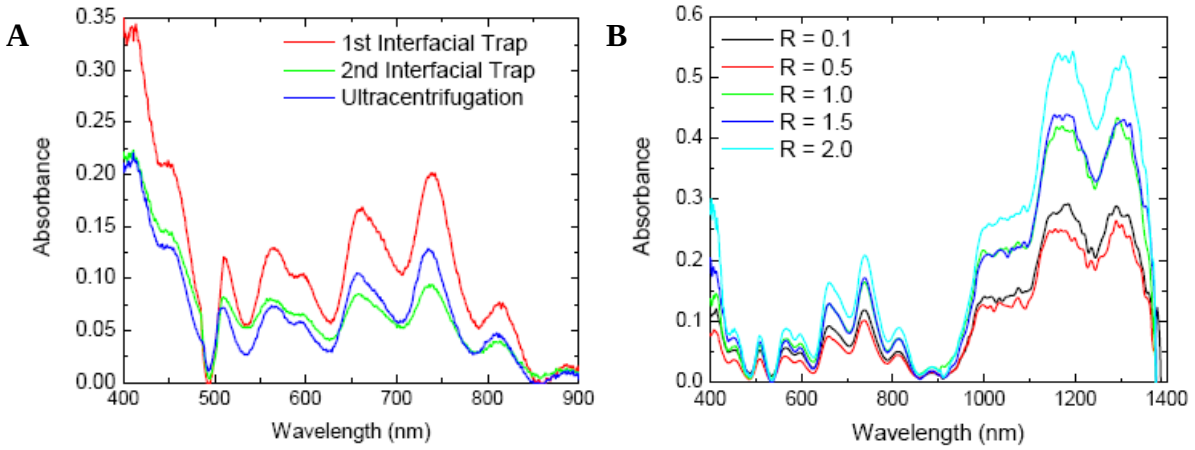

Figure A-2. A) Corrected absorbance of ultracentrifuged, single and two-step interfacial trapped SWNT suspensions after subtracting the non-resonant background. B) Corrected absorbance of interfacial trapped SWNT suspensions at different oil-to-aqueous volume ratios after subtracting the non-resonant background.

APPENDIX B
SUPPORTING INFORMATION FOR SOLVATOCHROMISM OF SWNTS

B.1 Measured solvatochromic shifts

Figures B-1 (A) and B-1 (B) show the fluorescence emission spectra of SWNTs excited with a 662 and 784 nm laser, respectively, in various nonpolar solvent microenvironments. All features of the spectra show solvatochromic shifts as well as intensity changes with each solvent microenvironment. Figure B-1 (C) is the absorbance spectra of SWNTs in the same solvent microenvironments. The spectra of SWNTs shows similar solvatochromic shifts; however, the E_{11} (0.85 – 1.4 eV) transitions of the SWNTs are more sensitive to the solvents (larger shifts) than the E_{22} (1.4 – 2.1 eV) transitions. Figure B-1 (D) shows the fluorescence emission spectra of SWNTs in a hexane/ODCB mixture at different mole fractions. The spectra show smooth changes to both the peak position and intensity.

B.2 Deconvolution of the spectra

SWNT fluorescence spectra contains information on the E_{11} interband transitions for each (n, m) SWNT type. All fluorescence spectra were deconvoluted into their respective bands for each (n, m) type using the Applied Nanospectrolyzer software (Houston, TX). The deconvolution routine uses Voigt profiles for each (n, m) peak. Changes to the position (E_{11}) and width of each (n, m) peak were limited to 0.1% and 3%, respectively, for each iteration to prevent the misidentification of peaks. After several iterations, the mean standard deviation (MSD) between the simulated and experimental data points was smaller than 0.005 (MSD < 0.005). Figure B-2 shows a typical simulated curve (red) compared to the experimental curve (blue) as well as the deconvoluted peaks corresponding to each (n, m) type. The simulated curve shows a good fit to the experimental curve. The peaks for each (n, m) component are shown under the simulated curve. The peak position of every (n, m) type of SWNTs after deconvolution is used in the

nonlinear optimization model described below. Note that the attached solvent characterization sheets show the deconvolution for all fluorescence spectra.

B.3 Nonlinear optimization model

The solvatochromic shifts of the interband transitions of SWNTs in each nonpolar solvent is given by the polarizability–polarizability interactions [98, 112]:

$$\Delta E_{11} = E_{11}^{air} - E_{11}^{solvent} = -C_{solvent} \frac{\Delta\alpha_{11}}{\beta\gamma a^3} \Delta f_{air-solvent} \tag{B-1}$$

where $C_{solvent}$ is a fluctuation parameter associated with SWNT dispersion forces, $\Delta\alpha_{11}$ is the change in polarizability of SWNTs between the ground and excited states, β is a shape factor for the SWNT, γ is a parameter associated with the location of the SWNT dipole in the volume a^3, and Δf is the solvent induction polarization given by $f(\eta^2) = 2(\eta^2 - 1)/(2\eta^2 + 1)$. The difference in SWNT polarizability, $\Delta\alpha_{11}$, used in equation (B-1) is assumed to be the longitudinal polarizability of the exciton (i.e., $\Delta\alpha_{11} \approx \alpha_{11,||}$) [110]. The longitudinal polarizability of each SWNT (n, m) type is assumed to be a function of the form, $\alpha_{11,||} = kR^a E_{11}^b$, where k is a constant, R is the SWNT radius, E_{11} is the band gap as measured in air, and a and b are integers. *[106-109]* The reaction field volume is assumed to have a radius equivalent to the SWNT radius and the constants $C_{solvent}$, k, β, and γ are combined into one constant $D_{solvent}$ to yield:

$$\Delta E_{11} = -D_{solvent} R^{a-3} E_{11}^b \Delta f \tag{B-2}$$

All fluorescence spectra were deconvoluted into their respective (n, m) peaks as described above. The E_{11} transitions for each (n, m) SWNT type were recorded from each spectrum in each solvent and subtracted from the E_{11} in air to give the solvatochromic shift (ΔE_{11}). The optical transitions in air were based on the equation [110]:

$$E_{11} = \frac{1241}{A_1 + A_2 d} + A_3 \frac{\cos(3\theta)}{d^2} \quad \text{(B-3)}$$

where A_1 and A_2 are 61.1 nm and 1113.6. A_3 depends on the chirality of the nanotubes expressed as mod ((n-m), 3) = j. For E_{11} transitions, A_3 is –0.077 and 0.032 eV nm^2 for j equal to 1 and 2, respectively.

As shown in Figure B-2, there can be considerable overlap in the deconvoluted fluorescence spectra for each (n, m) SWNT type. For example, the (7, 6) SWNT type shown in Figure B-2 (A) has good intensity and little overlap with other (n, m) SWNT types. On the other hand, the (12, 2) SWNT type in Figure B-1 (B) shows considerable overlap with other (n, m) types and low intensity. Obviously, more confidence should be assigned to those peaks that are well resolved and give intense fluorescence emission, such as the (7, 6) SWNT type. To account for the varying confidence levels in each deconvoluted peak, weighting factors were assigned based on the relative intensity ($w_{Intensity}$) and amount of overlap ($w_{Overlap}$) in each solvent. This technique is often used in nonlinear optimization to account for the relative importance of data. [114, 120] As shown in Table B-2, both the intensity and overlap were broken up into three categories and assigned values of 1, 0.5, or 0.25. Figure B-2 shows some examples of those peaks associated with each category. These two weighting factors were multiplied together to get the weighting factors listed in Table B-1 for all SWNT types in all solvents. The general trend shown in the table is that the (7, 6) and (7, 5) spectra have the highest confidence while the (9, 4) and (12, 1) have the lowest in each solvent.

A nonlinear optimization model was then formulated based on the fluorescence spectra with the objective function (ϕ) equal to the squared sum of residuals multiplied by the weighting factors (w_i):

$$\min \phi = \sum^{\text{all solvents}} \sum^{\text{all } n,m} w_{Intensity}^{n,m} w_{Overlap}^{n,m} \left(\Delta E_{11,measured}^{n,m} - \Delta E_{11,calculated}^{n,m} \right)^2 \qquad \text{(B-4)}$$

where ΔE_{11} are the measured values from Figure 5-5 subtracted from equation (B-4), or the calculated values from equation (B-2). These residuals were summed over all (n, m) types and solvents. The objective function was minimized using the generalized reduced gradient (GRG) method [114]. The values of all constants were constrained to values between –10 and 10 to aid optimization. The global parameters a and b had the additional constraints of being integers. Central differences were used to calculate the partial derivatives of the objective function. The search direction was determined at each iteration by using the conjugate method. The objective function was considered to converge once the relative change between iterations was less than 10^{-7}. A minimum of four different initial starting points for the parameters were used to obtain the global minimum rather than local minima.

In addition to the solution for all solvents, each solvent was solved independently to obtain the parameters a, b, and $D_{solvent}$. Table B-3 shows the results from all optimization calculations. Some optimization models had minima that were weak functions of the parameters a and b. In other words, the values of a and b could be changed by ±1 without affecting the value of the objective function. For example, the optimization of only heptane gave solutions of $a = -2$, $b = -3$ and $a = -3$, $b = -4$. However, one of these solutions coincided with the global optimization solution. Therefore, this data set was listed in Table B-3. Nearly all optimization solutions yielded solutions of $a = -2$ and $b = -3$. As seen in Table B-3, a global solution with all weighting factors set equal to 1 gave a different solution. However, as described above, this solution is discarded because of the difference in data quality for each (n, m) SWNT type.

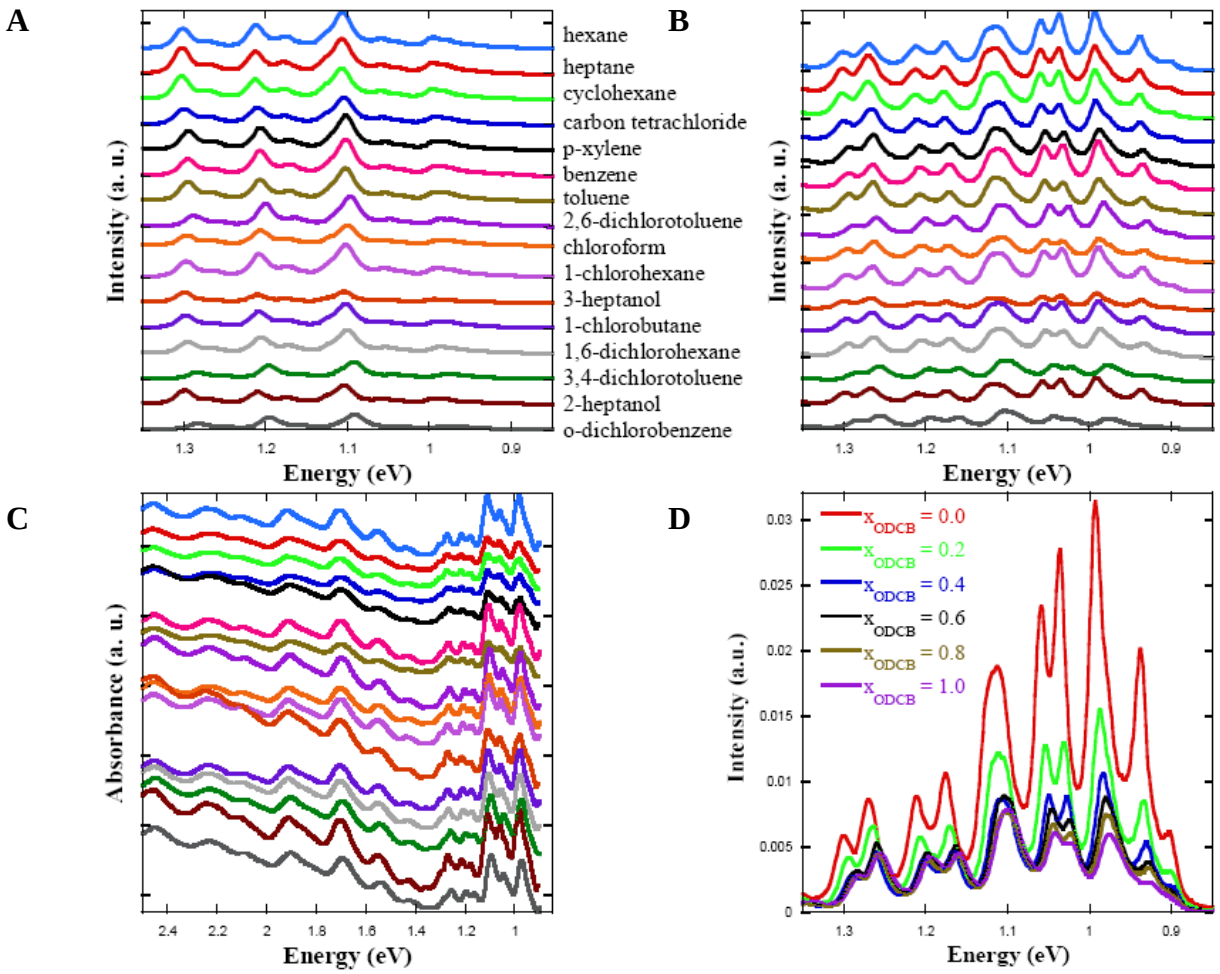

Figure B-1. PL emission spectra of SWNTs excited at A) 662 and B) 784 nm and C) absorbance spectra of SWNTs in nonpolar microenvironments. D) PL emission spectra (Ex. = 784 nm) of SWNTs in various hexane/ODCB mixture microenvironments. All spectra in a-c are offset for clarity and arranged by dielectric constant.

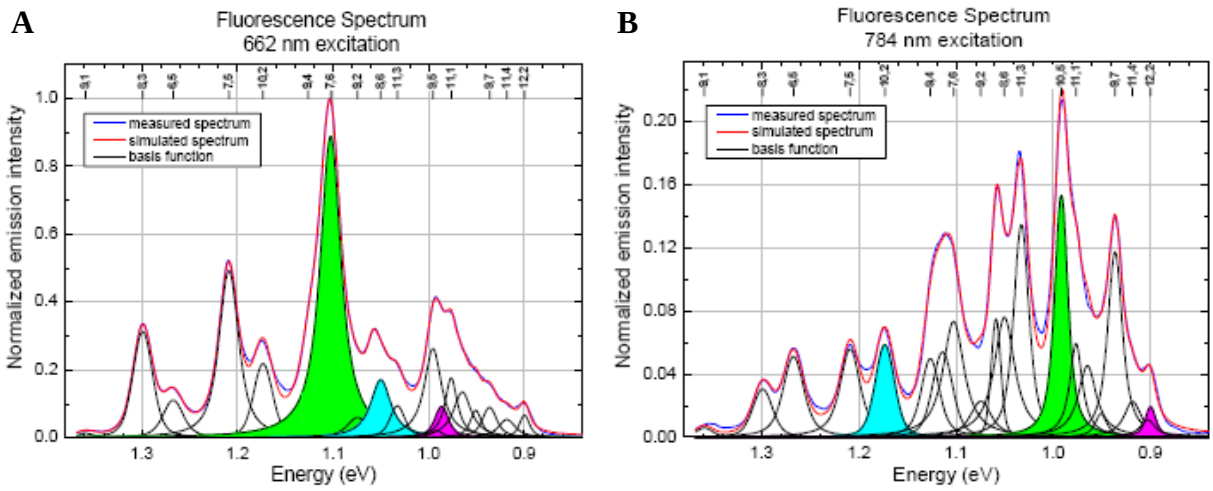

Figure B-2. Deconvolution of PL emission spectra for excitation at A) 662 and B) 784 nm. Weighting factors were assigned to each peak based on the amount of overlap with other peaks and the intensity. Those peaks highlighted in A) show examples of the three weighting factors associated with overlap while B) shows those associated with intensity. The green, blue, and purple curves were assigned values of 1, 0.5, and 0.25, respectively.

Table B-1. Criterion for assigning the weighting factors for both intensity and amount of overlap with other peaks.

Weighting Factor	Area Overlap	Intensity (662 nm excitation)	Intensity (784 nm excitation)
1	< 50%	> 0.4	> 0.08
0.5	between 50 and 100%	between 0.2 and 0.4	between 0.04 and 0.08
0.25	100%	< 0.2	< 0.04

Table B-2. Combined weighting factors ($w = w_{Intensity} - w_{Overlap}$) assigned for each ($n$,$m$) type as a function of solvent.

solvent	(6,5)	(8,3)	(7,5)	(7,6)	(10,2)	(9,4)	(11,1)	(8,6)	(9,5)	(12,1)	(11,3)	(12,2)	(10,5)	(9,7)
hexane	0.5	0.5	1	1	0.5	0.25	0.25	0.25	0.5	0.25	1	0.25	1	1
heptane	0.5	1	1	1	0.5	0.25	0.25	0.25	0.5	0.5	1	0.25	1	1
cyclohexane	0.5	1	1	1	0.5	0.25	0.25	0.25	0.5	0.5	1	0.25	1	1
carbon tetrachloride	0.5	0.5	1	1	0.5	0.25	0.25	0.25	0.5	0.25	1	0.25	1	1
p-xylene	0.5	0.5	1	1	0.5	0.0625	0.25	0.25	0.5	0.125	1	0.25	1	0.5
benzene	0.5	0.5	1	1	0.5	0.125	0.25	0.5	0.5	0.125	1	0.25	1	1
toluene	0.5	0.5	1	1	0.5	0.125	0.25	0.5	0.5	0.125	1	0.25	1	0.5
2,6-dichlorotoluene	0.5	0.5	0.5	1	0.5	0.125	0.0625	0.5	0.0625	0.0625	1	0.25	0.25	0.5
chloroform	0.5	0.5	1	1	0.5	0.125	0.25	0.5	0.125	0.125	0.5	0.25	0.25	1
1-chlorohexane	0.5	0.5	1	1	0.5	0.125	0.25	0.5	0.125	0.125	1	0.25	0.5	1
3-heptanol	0.5	0.5	1	1	0.5	0.25	0.25	0.25	0.5	0.25	1	0.25	1	1
1-chlorobutane	0.5	0.5	1	1	0.5	0.125	0.25	0.5	0.125	0.125	1	0.25	0.5	1
1,6-dichlorohexane	0.5	0.5	1	1	0.5	0.125	0.25	0.5	0.125	0.0625	0.5	0.25	0.25	1
3,4-dichlorotoluene	0.5	0.5	1	1	0.5	0.0625	0.25	0.5	0.25	0.0625	0.25	0.125	-	0.0625
2-heptanol	0.5	0.5	1	1	0.5	0.25	0.25	0.25	0.5	0.25	1	0.25	1	1
o-dichlorobenzene	0.5	0.5	1	1	0.5	0.125	0.25	0.5	0.125	0.0625	0.25	0.125	0.25	-
average	**0.50**	**0.56**	**0.97**	**1.00**	**0.50**	**0.16**	**0.24**	**0.39**	**0.34**	**0.19**	**0.84**	**0.23**	**0.73**	**0.84**

Table B-3. Optimization results for all fitted parameters when solved as individual systems and collectively.

Parameter[1]	All solvents	solvent																All solvents ($w_i = 1$)[4]
		hexane	heptane[2]	cyclohexane[2]	carbon tetrachloride	p-xylene[3]	benzene	toluene	2,6-dichlorotoluene	chloroform	1-chlorohexane	3-heptanol	1-chlorobutane	1,6-dichlorohexane[3]	3,4-dichlrotoluene	2-heptanol	o-dichlorobenzene	
a	-2	-2	-2	-2	-2	-2	-2	-2	0	-2	-2	-3	-2	-2	0	-3	-1	-3
b	-3	-3	-3	-3	-3	-3	-3	-3	-1	-3	-3	-4	-3	-3	-1	-4	-2	-4
D_{hexane}	4.1	4.1																2.2
D_{heptane}	3.9		3.9															2.1
$D_{\text{cyclohexane}}$	3.6			3.6														1.9
$D_{\text{carbon tetrachloride}}$	3.6				3.6													1.9
$D_{\text{p-xylene}}$	3.6					3.6												1.9
D_{benzene}	3.6						3.6											1.9
D_{toluene}	3.6							3.6										1.9
$D_{\text{2,6-dichlorotoluene}}$	3.6								13.3									1.8
$D_{\text{chloroform}}$	3.9									3.9								2.0
$D_{\text{1-chlorohexane}}$	4.0										4.0							2.1
$D_{\text{3-heptanol}}$	3.8											2.0						2.0
$D_{\text{1-chlorobutane}}$	4.1												4.1					2.2
$D_{\text{1,6-dichlorohexae}}$	3.9													3.9				2.0
$D_{\text{3,4-dichlorotoluene}}$	3.9														14.4			1.9
$D_{\text{2-heptanol}}$	3.8															2.0		2.0
$D_{\text{o-dichlorobenzene}}$	3.9																7.5	2.0

[1] D is given in meV·nm^5·eV^3.

[2] Minimum was weak function and also gave a possible solution of $a = -3$ and $b = -4$. The listed solution was chosen since it was identical to the overall optimization parameter set for all solvents.

[3] Minimum was weak function and also gave a possible solution of $a = -1$ and $b = -2$. The listed solution was chosen since it was identical to the overall optimization parameter set for all solvents.

[4] Optimization solution with all weighting factors set to 1. This solution is not recommended given the uncertainty in the deconvolution.

LIST OF REFERENCES

[1] P. G. Collins, P. Avouris, *Sci. Am.* **2000**, 62.

[2] S. M. Bachilo, M. S. Strano, C. Kittrell, R. H. Hauge, R. E. Smalley, R. B. Weisman, *Science* **2002**, *298*, 2361.

[3] M. S. Dresselhaus, G. Dresselhaus, A. Jorio, A. G. Souza Filho, M. A. Pimenta, R. Saito, *Acc. Chem. Res.* **2002**, *35*, 1070.

[4] M. S. Dresselhaus, G. Dresselhaus, P. C. Eklund, *Science of Fullerenes and Carbon Nanotubes*, Academic Press, San Diego, CA **1996**.

[5] R. Saito, G. Dresselhaus, M. S. Dresselhaus, *Physical Properties of Carbon Nanotubes*, Imperial College Press, London **1998**.

[6] T. W. Odom, J. L. Huang, P. Kim, C. M. Lieber, *Nature* **1998**, *391*, 62.

[7] J. Kong, N. R. Franklin, C. Zhou, M. G. Chapline, S. Peng, K. Cho, H. Dai, *Science* **2000**, *287*, 622.

[8] L. A. Girifalco, M. Hodak, R. S. Lee, *Phys. Rev. B* **2000**, *62*, 13104.

[9] M. O'Connell, S. M. Bachilo, C. Huffman, V. C. Moore, M. S. Strano, E. Haroz, K. L. Rialon, P. Boul, W. H. Noon, C. Kittrell, J. Ma, R. H. Hauge, R. B. Weisman, R. Smalley, *Science* **2002**, *297*, 593.

[10] M. Jones, C. Engtrakul, W. K. Metzger, R. J. Ellingson, A. J. Nozik, M. J. Heben, G. Rumbles, *Phys. Rev. B* **2005**, *71*, 115426.

[11] B. J. Landi, H. J. Ruf, J. J. Worman, R. P. Raffaelle, *J. Phys. Chem. B* **2004**, *108*, 17089.

[12] A. M. Rao, E. Richter, S. Bandow, B. Chase, P. C. Eklund, K. A. Williams, S. Fang, K. R. Subbaswamy, M. Menon, A. Thess, R. E. Smalley, G. Dresselhaus, M. S. Dresselhaus, *Science* **1997**, *275*, 187.

[13] D. A. Heller, P. W. Barone, J. P. Swanson, R. M. Mayrhofer, M. S. Strano, *J. Phys. Chem. B* **2004**, *108*, 6905.

[14] J. A. Fagan, B. J. Landi, I. Mandelbaum, J. R. Simpson, V. Bajpai, B. J. Bauer, K. Migler, A. R. Hight Walker, R. Raffaelle, E. K. Hobbie, *J. Phys. Chem. B* **2006**, *110*, 23801.

[15] V. C. Moore, M. S. Strano, E. H. Haroz, R. H. Hauge, R. E. Smalley, *Nano Lett.* **2003**, *3*, 1379.

[16] M. S. Strano, V. C. Moore, M. K. Miller, M. J. Allen, E. H. Haroz, C. Kittrell, R. H. Hauge, R. E. Smalley, *J. Nanosci. Nanotech.* **2003**, *3*, 81.

[17] M. F. Islam, E. Rojas, D. M. Bergey, A. T. Johnson, A. G. Yodh, *Nano Lett.* **2003**, *3*, 269.

[18] K. Yurekli, C. A. Mitchell, R. J. Krishnamoorti, *J. Am. Chem. Soc.* **2004**, *126*, 9902.

[19] R. Bandyopadhyaya, E. Nativ-Roth, O. Regev, R. Yerushalmi-Rozen, *Nano Lett.* **2002**, *2*, 25.

[20] E. J. Wallace, M. S. P. Sansom, *Nano Lett.* **2007**, *7*, 1923.

[21] S. U. Pickering, *J. Chem. Soc, Trans.* **1907**, *91*, 2001.

[22] Y. Lin, H. Skaff, T. Emrick, A. D. Dinsmore, T. P. Russell, *Science* **2003**, *299*, 226.

[23] J. He, Q. Zhang, S. Gupta, T. Emrick, T. R. Russell, P. Thiyagarajan, *Small* **2007**, *3*, 1214.

[24] P. Jauregi, M. A. Hoeben, R. G. J. M. van der Lans, G. Kwant, L. A. M. van der Wielen, *Ind. Eng. Chem. Res.* **2001**, *40*, 5815.

[25] H. F. Lu, B. Fei, J. H. Xin, R. H. Wang, L. Li, W. C. Guan, *Carbon* **2007**, *45*, 936.

[26] B. P. Binks, J. H. Clint, *Langmuir* **2002**, *18*, 1270.

[27] R. Krupke, F. Hennrich, H. von Lohneysen, M. M. Kappes, *Science* **2003**, *301*, 344.

[28] Z. H. Chen, X. Du, M. H. Du, C. D. Rancken, H. P. Cheng, A. G. Rinzler, *Nano Lett.* **2003**, *3*, 1245.

[29] M. Zheng, A. Jagota, M. S. Strano, A. P. Santos, P. Barone, S. G. Chou, B. A. Diner, M. S. Dresselhaus, R. S. McLean, G. B. Onoa, G. G. Samsonidze, E. D. Semke, M. Usrey, D. J. Walls, *Science* **2003**, *302*, 1545.

[30] M. S. Arnold, A. A. Green, J. F. Hulvat, S. I. Stupp, M. C. Hersam, *Nature Nanotech.* **2006**, *1*, 60.

[31] K. J. Ziegler, *Trends Biotechnol.* **2005**, *23*, 440.

[32] P. W. Barone, S. Baik, D. A. Heller, M. S. Strano, *Nature Mater.* **2005**, *4*, 86.

[33] Z. Yao, C. L. Kane, C. Dekker, *Phys. Rev. Lett.* **2000**, *84*, 2941.

[34] R. K. Wang, R. D. Reeves, K. J. Ziegler, *J. Am. Chem. Soc.* **2007**, *129*, 15124.

[35] R. Shvartzman-Cohen, E. Nativ-Roth, E. Baskaran, Y. Levi-Kalisman, I. Szleifer, R. Yerushalmi-Rozen, *J. Am. Chem. Soc.* **2004**, *126*, 14850.

[36] J. L. Bahr, E. T. Mickelson, M. J. Bronikowski, R. E. Smalley, J. M. Tour, *Chem. Commun.* **2001**, 193.

[37] T. Rueckes, K. Kim, E. Joselevich, G. Y. Tseng, C.-L. Cheung, C. M. Lieber, *Science* **2000**, *289*, 94.

[38] S. Banerjee, T. Hemraj-Benny, S. S. Wong, *Adv. Mater.* **2005**, *17*, 17.

[39] A. Hirsch, *Angew. Chem. Int. Ed.* **2002**, *41*, 1853.

[40] V. N. Khabashesku, W. E. Billups, J. L. Margrave, *Accounts Chem. Res.* **2002**, *35*, 1087.

[41] P. M. Ajayan, J. M. Tour, *Nature* **2007**, *447*, 1066.

[42] C. W. Lee, C.-H. Weng, L. Wei, Y. Chen, M. B. Chan-Park, C.-H. Tsai, K.-C. Leou, C. H. P. Poa, M. Glerup, J. Wang, L.-J. Li, *J. Phys. Chem. C* **2008**, *112*, 12089.

[43] P. Jauregi, M. A. Hoeben, R. G. J. M. van der Lans, G. Kwant, L. A. M. van der Wielen, *Biotechnol. Bioeng.* **2002**, *78*, 355.

[44] M. A. Hoeben, R. G. J. M. van der Lans, L. A. M. van der Wielen, G. Kwant, *AIChE J.* **2004**, *50*, 1156.

[45] H. Wang, E. K. Hobbie, *Langmuir* **2003**, *19*, 3091.

[46] E. K. Hobbie, B. J. Bauer, J. Stephens, M. L. Becker, P. McGuiggan, S. D. Hudson, H. Wang, *Langmuir* **2005**, *21*, 10284.

[47] K. J. Ziegler, D. J. Schmidt, U. Rauwald, K. N. Shah, E. L. Flor, R. H. Hauge, R. E. Smalley, *Nano Lett.* **2005**, *5*, 2355.

[48] P. Asuri, S. S. Karajanagi, J. S. Dordick, R. S. Kane, *J. Am. Chem. Soc.* **2006**, *128*, 1046.

[49] A. Menner, R. Verdejo, M. Shaffer, A. Bismarck, *Langmuir* **2007**, *23*, 2398.

[50] M. i. h. Panhuis, V. N. Paunov, *Chem. Commun.* **2005**, 1726.

[51] H. Yi, H. Song, X. Chen, *Langmuir* **2007**, *23*, 3199.

[52] K. J. Ziegler, U. Rauwald, Z. Gu, F. Liang, W. E. Billups, R. H. Hauge, R. E. Smalley, *J. Nanosci. Nanotech* **2007**, *7*, 2917.

[53] E. I. Yaseen, T. J. Herald, F. M. Aramouni, S. Alavi, *Food Research International* **2005**, *38*, 111.

[54] C. Sanchez, D. Renard, P. Robert, C. Schmitt, J. Lefebvre, *Food Hydrocolloids* **2002**, *16*, 257.

[55] A. N. G. Parra-Vasquez, I. Stepanek, V. A. Davis, V. C. Moore, E. H. Haroz, J. Shaver, R. H. Hauge, R. E. Smalley, M. Pasquali, *Macromolecules* **2007**, *40*, 4043.

[56] Y. Tan, D. E. Resasco, *J. Phys. Chem. B* **2005**, *109*, 14454.

[57] H. Qian, C. Georgi, N. Anderson, A. A. Green, M. C. Hersam, L. Novotny, A. Hartschuh, *Nano Lett.* **2008**, *8*, 1363.

[58] P. H. Tan, A. G. Rozhin, T. Hasan, P. Hu, V. Scardaci, W. I. Milne, A. C. Ferrari, *Phys. Rev. Lett.* **2007**, *99*, 137402.

[59] O. N. M. Torrens, D. E.; Zheng, M.; Kikkawa, J. M., *Nano Lett.* **2006**, *6*, 2864.

[60] R. A. Graff, J. P. Swanson, P. W. Barone, S. Baik, D. A. Heller, M. S. Strano, *Adv. Mater.* **2005**, *17*, 980.

[61] M. J. O'Connell, S. Sivaram, S. K. Doorn, *Phys. Rev. B* **2004**, *69*, 235415.

[62] W. Zhou, M. F. Islam, H. Wang, D. L. Ho, A. G. Yodh, K. I. Winey, J. E. Fischer, *Chem. Phys. Lett.* **2004**, *384*, 185.

[63] H. Wang, W. Zhou, D. L. Ho, K. I. Winey, J. E. Fischer, C. J. Glinka, E. K. Hobbie, *Nano Lett.* **2004**, *4*, 1789.

[64] B. P. Binks, S. O. Lumsdon, *Langmuir* **2000**, *16*, 8622.

[65] V. N. Manoharan, *Solid State Commun.* **2006**, *139*, 557.

[66] P. Cherukuri, S. M. Bachilo, S. H. Litovsky, R. B. Weisman, *J. Am. Chem. Soc.* **2004**, *126*, 15638.

[67] T. K. Leeuw, R. M. Reith, R. A. Simonette, M. E. Harden, P. Cherukuri, D. A. Tsyboulski, K. M. Beckingham, R. B. Weisman, *Nano Lett.* **2007**, *7*, 2650.

[68] P. W. Barone, R. S. Parker, M. S. Strano, *Anal. Chem.* **2005**, *77*, 7556.

[69] D. A. Heller, H. Jin, B. M. Martinez, D. Patel, B. M. Miller, T. K. Yeung, P. V. Jena, C. Hobartner, T. Ha, S. K. Silverman, M. S. Strano, *Nature Nanotech.* **2009**, *4*, 114.

[70] S. D. Bergin, V. Nicolosi, P. V. Streich, S. Giordani, Z. Y. Sun, A. H. Windle, P. Ryan, N. P. Niraj, Z. T. Wang, L. Carpenter, W. J. Blau, J. J. Boland, J. P. Hamilton, J. N. Coleman, *Adv. Mater.* **2008**, *20*, 1876.

[71] R. Haggenmueller, S. S. Rahatekar, J. A. Fagan, J. H. Chun, M. L. Becker, R. R. Naik, T. Krauss, L. Carlson, J. F. Kadla, P. C. Trulove, D. F. Fox, H. C. DeLong, Z. C. Fang, S. O. Kelley, J. W. Gilman, *Langmuir* **2008**, *24*, 5070.

[72] R. K. Wang, H.-O. Park, W.-C. Chen, C. Silvera-Batista, R. D. Reeves, J. E. Butler, K. J. Ziegler, *J. Am. Chem. Soc.* **2008**, *130*, 14721.

[73] L. Vaisman, H. D. Wagner, G. Marom, *Adv. Coll. Inter. Sci.* **2006**, *128-130*, 37.

[74] B. White, S. Banerjee, S. O'Brien, N. J. Turro, I. P. Herman, *J. Phys. Chem. C* **2007**, *111*, 13684.

[75] Z. Sun, V. Nicolosi, D. Rickard, S. D. Bergin, D. Aherne, J. N. Coleman, *J. Phys. Chem. C* **2008**, *112*, 10692.

[76] R. K. Wang, W.-C. Chen, D. K. Campos, K. J. Ziegler, *J. Am. Chem. Soc.* **2008**, *130*, 16330.

[77] A. Ishibashi, N. Nakashima, *Chem. Eur. J.* **2006**, *12*, 7595.

[78] T. Okazaki, T. Saito, K. Matsuura, S. Ohshima, M. Yumura, S. Iijima, *Nano Lett.* **2005**, *5*, 2618.

[79] T. Kato, R. Hatakeyama, *J. Am. Chem. Soc.* **2008**, *130*, 8101.

[80] J. Lefebvre, D. G. Austing, J. Bond, P. Finnie, *Nano Lett.* **2006**, *6*, 1603.

[81] R. J. Chen, Y. G. Zhan, D. W. Wang, H. J. Dai, *J. Am. Chem. Soc.* **2001**, *123*, 3838.

[82] P. Cherukuri, C. J. Gannon, T. K. Leeuw, H. K. Schmidt, R. E. Smalley, S. A. Curley, B. Weisman, *P. Natl. Acad. Sci. USA* **2006**, *103*, 18882.

[83] Y. Kang, T. A. Taton, *J. Am. Chem. Soc.* **2003**, *125*, 5650.

[84] Y. Dror, W. Pyckhout-Hintzen, Y. Cohen, *Macromolecules* **2005**, *38*, 7828.

[85] L. Cognet, D. A. Tsyboulski, J.-D. R. Rocha, C. D. Doyle, J. M. Tour, R. B. Weisman, *Science* **2007**, *316*, 1465.

[86] D. A. Tsyboulski, J. R. Rocha, S. M. Bachilo, L. Cognet, R. B. Weisman, *Nano Lett.* **2007**, *7*, 3080.

[87] T. Gokus, A. Hartschuh, H. Harutyunyan, M. Allegrini, F. Hennrich, M. Kappes, A. A. Green, M. C. Hersam, P. T. Araujo, A. Jorio, *Appl. Phys. Lett.* **2008**, *92*, 153116.

[88] M. S. Strano, C. B. Huffman, V. C. Moore, M. J. O'Connell, E. H. Haroz, J. Hubbard, M. Miller, K. Rialon, C. Kittrell, S. Ramesh, R. H. Hauge, R. E. Smalley, *J. Phys. Chem. B* **2003**, *107*, 6979.

[89] J. G. Duque, L. Cognet, A. N. G. Parra-Vasquez, N. Nicholas, H. K. Schmidt, M. Pasquali, *J. Am. Chem. Soc.* **2008**, *130*, 2626.

[90] G. Dukovic, B. E. White, Z. Y. Zhou, F. Wang, S. Jockusch, M. L. Steigerwald, T. F. Heinz, R. A. Friesner, N. J. Turro, L. E. Brus, *J. Am. Chem. Soc.* **2004**, *126*, 15269.

[91] J. L. Blackburn, T. J. McDonald, W. K. Metzger, C. Engtrakul, G. Rumbles, M. J. Heben, *Nano Lett.* **2008**, *8*, 1047.

[92] J. Crochet, M. Clemens, T. Hertel, *J. Am. Chem. Soc.* **2007**, *129*, 8058.

[93] D. A. Heller, R. M. Mayrhofer, S. Baik, Y. V. Grinkova, M. L. Usrey, M. S. Strano, *J. Am. Chem. Soc* **2004**, *126*, 14567.

[94] J. A. Fagan, J. R. Simpson, B. J. Bauer, S. H. De Paoli Lacerda, M. L. Becker, J. Chun, K. B. Migler, A. R. Hightwalker, E. K. Hobbie, *J. Am. Chem. Soc.* **2007**, *129*, 10607.

[95] M. J. O'Connell, P. Boul, L. M. Ericson, C. Huffman, Y. H. Wang, E. Haroz, C. Kuper, J. Tour, K. D. Ausman, R. E. Smalley, *Chem. Phys. Lett.* **2001**, *342*, 265.

[96] F. S. Wang, M. Y.; Huang, L.; Huang, X. M. H.; Wu, Y.; Kim, J.; Hone, J.; O'Brien, S.; Brus, L. E.; Heinz, T. F., *Phys. Rev. Lett.* **2006**, *96*, 167401.

[97] T. Nose, N. Numasawa, *Comput. Theor. Polm. Sci.* **2001**, *11*, 167.

[98] P. Suppan, N. Ghoneim, *Solvatochromism*, The Royal Society of Chemistry, Cambridge, UK **1997**.

[99] K. R. Moonoosawmy, P. Kruse, *J. Am. Chem. Soc.* **2008**, *130*, 13417.

[100] M. S. Dresselhaus, P. C. Eklund, *Adv. Phys.* **2000**, *49*, 705.

[101] W. Zhou, J. Vavro, N. M. Nemes, J. E. Fischer, F. Borondics, K. Kamaras, D. B. Tanner, *Phys. Rev. B* **2005**, *71*, 205423.

[102] T. J. McDonald, C. Engtrakul, M. Jones, G. Rumbles, M. J. Heben, *J. Phys. Chem. B.* **2006**, *110*, 25339.

[103] E. A. G. Aniansson, S. N. Wall, M. Almgren, H. Hoffmann, I. Kielmann, W. Ulbricht, R. Zana, J. Lang, C. Tondre, *J. Phys. Chem.* **1976**, *80*, 905.

[104] S. Arepalli, P. Nikolaev, O. Gorelik, V. G. Hadjiev, W. Holmes, L. Yowell, *Carbon* **2004**, *42*, 1783.

[105] N. R. Tummala, A. Striolo, *ACS Nano* **2009**, *3*, 595.

[106] L. X. Benedict, S. G. Louie, M. L. Cohen, *Phys. Rev. B* **1995**, *52*, 8541.

[107] E. N. Brothers, G. E. Scuseria, K. N. Kudin, *J. Phys. Chem. B* **2006**, *110*, 12860.

[108] B. Kozinsky, N. Marzari, *Phys. Rev. Lett.* **2006**, *96*, 166801.

[109] G. Y. Guo, K. C. Chu, D. S. Wang, C. G. Duan, *Comput. Mater. Sci.* **2004**, *30*, 269.

[110] J. H. Choi, M. S. Strano, *Appl. Phys. Lett.* **2007**, *90*, 223114+.

[111] M. S. Brown, J. W. Shan, C. Lin, F. M. Zimmermann, *Appl. Phys. Lett.* **2007**, *90*, 203108.

[112] P. Suppan, *J. Photoch. Photobio. A* **1990**, *50*, 293.

[113] T. H. Lowry, K. S. Richardson, Benjamin-Cummings Publishing Company, **1987**.

[114] S. Smith, L. Lasdon, *J. Comput.* **1992**, *4*, 1.

[115] D. R. Lide, *CRC Handbook of Chemistry and Physics. 80th Edition*, CRC Press.

[116] K. E. Calderbank, R. J. W. Le Fèvre, R. K. Pierens, *J. Chem. Soc.* **1969**, 968.

[117] W. E. Vaughan, National Academy of Sciences, Washington, DC **1975**.

[118] A. G. Ryabenko, T. V. Dorofeeva, G. I. Zvereva, *Carbon* **2004**, *42*, 1523.

[119] N. Nair, M. L. Usrey, W. J. Kim, R. D. Braatz, M. S. Strano, *Anal. Chem.* **2006**, *78*, 7689.

[120] K. J. Ziegler, J. Chlistunoff, L. Lasdon, K. P. Johnston, *Comput.Chem.* **1999**, *27*, 421.

BIOGRAPHICAL SKETCH

Randy Kai-Wei Wang grew up in Taipei, Taiwan. He received his Bachelor of Science degree from the Department of Chemical Engineering at the National Taiwan University in Taiwan in June 2003. He started his military service in July 2003 and he was discharged in February 2005. He began his graduate studies at the University of Florida in August 2005 and joined Professor Kirk J. Ziegler's nanoscale material research group to pursue a Doctor of Philosophy degree. He graduated in the summer of 2009 after spending four years being educated in chemical engineering and material science.